DOE/JPL 954350 - 78/3
Distribution Category UC-63

FLOATING SUBSTRATE PROCESS

Large-Area Silicon Sheet Task
Low-Cost Solar Array Project

FINAL REPORT

Subcontract No. 954350

by

M. Garfinkel, Program Manager
R.N. Hall, Principal Investigator

June 23, 1978

General Electric Company
Corporate Research and Development
P.O. Box 8
Schenectady, NY 12301

The JPL Low-cost Silicon Solar Array Project is sponsored by the U.S. Department of Energy and forms part of the Solar Photovoltaic Conversion Program to initiate a major effort toward the development of low-cost solar arrays. This work was performed for the Jet Propulsion Laboratory, California Institute of Technology by agreement between NASA and DOE.

SRD-78-015

ABSTRACT

The work presented in this report was directed toward the demonstration of the practical feasibility of the Floating Substrate Process for the growth of silicon sheet. Supercooling of silicon-tin alloy melts was studied. Values as high as 78 °C at 1100 °C and 39 °C at 1200 °C were observed, corresponding to supersaturation parameter values 0.025 and 0.053 at 1050 °C and 1150 °C, respectively. The interaction of tin with silane gas streams was investigated over the temperature range 1000 to 1200 °C. Single-pass conversion efficiencies exceeding 30% were obtained. The growth habit of spontaneously-nucleated surface growth was determined to be consistent with dendritic and web growth from <111> singly-twinned triangular nucleii. Surface growth of interlocking silicon crystals, thin enough to follow the surface of the liquid and with growth velocity as high as 5 mm/min, was obtained. Large area single-crystal growth along the melt surface was not achieved. Small single-crystal surface growth was obtained which did not propagate beyond a few millimeters. The probable reason for the polycrystalline growth is the poisoning of the growth interface by impurities.

TABLE OF CONTENTS

LIST OF ILLUSTRATIONS

LIST OF ILLUSTRATIONS (CONT'D)

LIST OF ILLUSTRATIONS (CONT'D)

LIST OF ILLUSTRATIONS (CONT'D)

LIST OF TABLES

LIST OF TABLES (CONT'D)

Section I

INTRODUCTION AND GENERAL DESCRIPTION

Chemical vapor deposition (CVD) has been widely used to produce thin films on silicon substrates. A similar deposition process was proposed as a means of generating thin single-crystal sheets of silicon that are supported by flotation upon the surface of a pool of liquid metal. Most of the growth was to take place near one end of the pool where the temperature is sufficiently high (~1200 °C) for rapid silicon deposition to take place. The arriving silicon dissolves in the liquid metal until the metal becomes saturated and then starts to crystallize on the surface. Under steady-state growth conditions the silicon sheet is drawn toward the cooler end of the furnace, where it may be lifted off the supporting liquid after its temperature has dropped below the range of plastic deformation. This growth process is illustrated schematically in Figure 1.

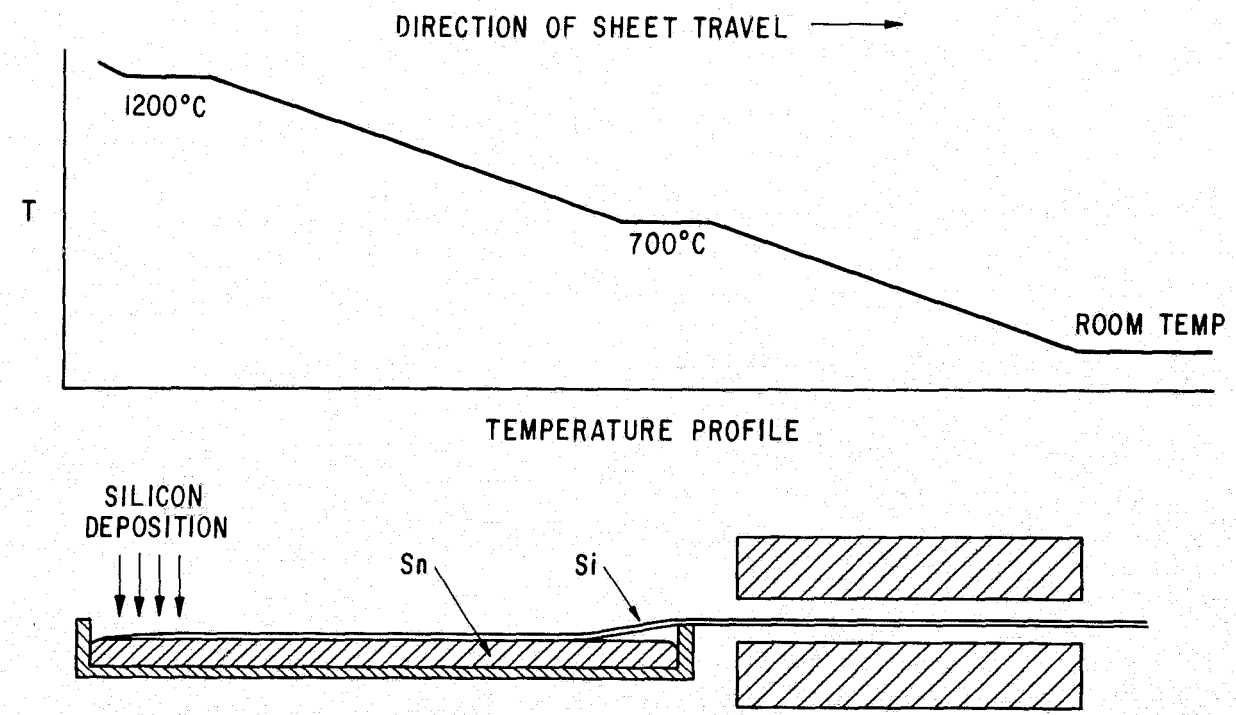

Figure 1. Floating Silicon Substrate Sheet Growth

Growth conditions at the edge of the sheet are similar to those of Czochralski or ribbon growth from the melt, except the driving force for crystallization is not supercooling but, rather, supersaturation at the surface of the liquid metal caused by the vapor deposition of silicon. The relationship between supercooling and supersaturation may be seen in Figure 1a which is the liquidus for the tin-silicon system in the region of interest. One

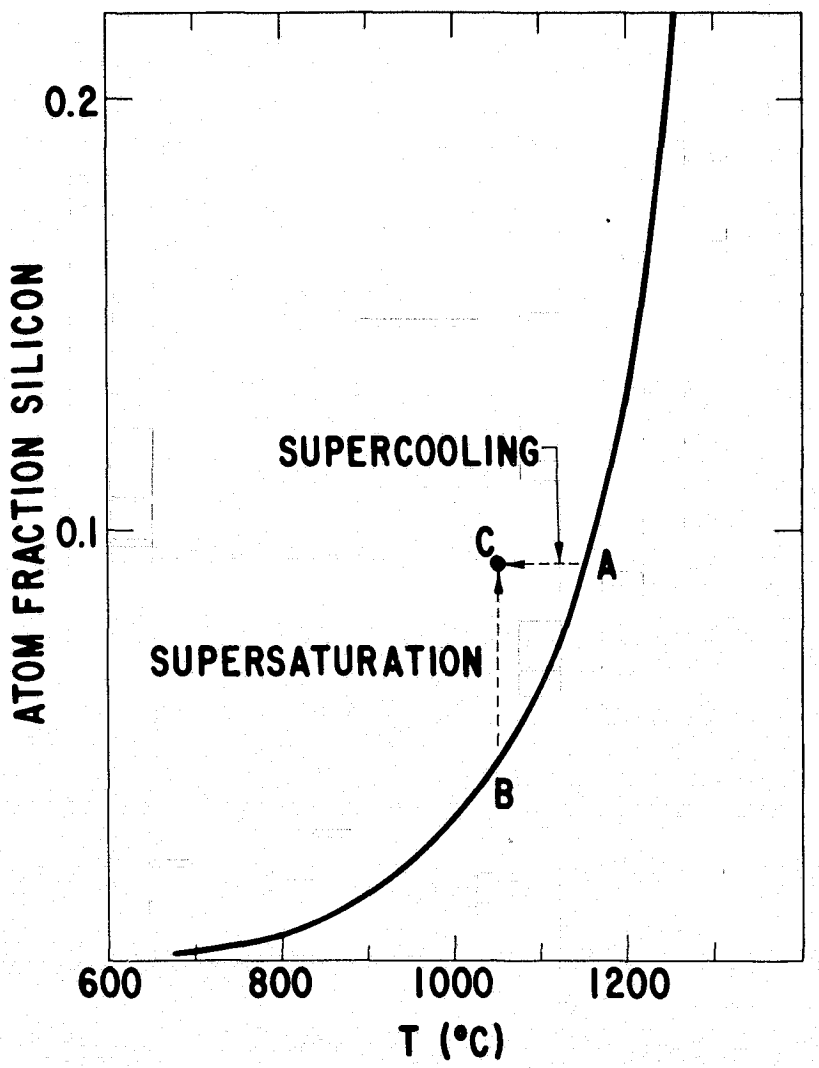

Figure 1a. Silicon-Tin Liquidus

may arrive at the supersaturated point C either by supercooling from A or by introducing additional silicon starting at point B. As a consequence, the edge of the sheet advances until it reaches a steady-state location near the boundary of the deposition zone. The sheet grows in thickness by vapor phase epitaxial deposition on crystalline silicon as it travels through the vapor deposition zone. Thus its thickness can be adjusted to the desired value by controlling the length of this zone and/or the flow rates of the vapor phase constituents.

Tin is a suitable metal to use as the supporting liquid because of its low vapor pressure and lack of electrical activity as an impurity in silicon. The liquid metal will be saturated with silicon by contact with the overlying sheet throughout the length of the pool. Under conditions where the silicon sheet and not the liquid is transported at a rate slow enough for the dissolved silicon to diffuse to the bottom of the container, there

will be no appreciable growth by liquid phase epitaxial (LPE) deposition upon the lower surface of the silicon sheet. For this reason the choice of liquid is not restricted to inactive elements but could be a nonvolatile metal such as indium or lead.

An attractive feature of floating substrate growth is the gettering action of the liquid metal, which ensures the removal of fast diffusing, deep-level impurities whose presence would otherwise degrade the lifetime of the silicon and lower its photovoltaic efficiency. Such impurities commonly are present in diffused junctions but can be eliminated in the present approach to solar cells because a subsequent diffusion process is not required. To prevent deep-level impurities from accumulating, it is necessary to provide for a gradual replenishment of the liquid in the pool by drawing it off at the cool end and replacing it with clean metal at the hot end.

The principal features of the floating substrate growth process that are still unresolved at the end of the present contract effort are phenomena that take place at the growing edge of the sheet. It was anticipated that once nucleated as a single-crystal sheet, growth would continue up to the forward boundary of the deposition zone, much like a two-dimensional analog of Bridgeman or Czochralski growth. The growth velocity should not be limited by the heat of solidification generated by the growing sheet because of the large area over which growth takes place and the excellent thermal contact that exists between the sheet and the metal pool. Growth at the leading edge does not take place by deposition of silicon from the underlying liquid but, rather, should be fed by the arrival of vapor deposited silicon within a thin surface layer. Therefore, the concentration of silicon within the liquid metal should be maintained close to its saturation solubility at the corresponding temperature, and there is no requirement that silicon be transported any appreciable distance through the liquid. Consequently, the growth velocity should not be seriously limited by diffusion within the liquid, as is the case with rapid LPE growth.

The principal factor that determines the rate of production of the silicon sheet appears to be the time required for obtaining the desired sheet thickness by vapor phase epitaxial growth. For example, assuming a deposition rate of 12.5 μm/min and a deposition zone 20 cm in length, a 100-μm-thick sheet could be grown at a production rate of 2.5 cm/min.

The floating substrate process does not involve intrinsic growth parameters that would limit the width of the sheet. Therefore, its dimensions can be determined in accord with the needs of the subsequent processing steps. Efficient growth requires that the width be at least several centimeters (because of allowance along either side of the sheet for restricting lateral growth in order to prevent contact with the sides of the tray). Also, the edges of the sheet will be tapered over a distance of several millimeters and will probably need to be trimmed. A sheet width of about 10 cm would appear to be a reasonable choice.

The process should be well adapted to continuous operation. The feed materials are gases and liquids and the output sheet can either be fed directly to the next step in automated cell production, accumulated on rolls, or cut to convenient lengths and stacked for shipment. The unreacted gaseous components that emerge from the deposition chamber can be separated, purified, and returned to the cycle using the same technology as in present silicon manufacture or upgraded as through the results of silicon material task findings. Because there is a minimum requirement for mechanical manipulation or precision control, each furnace can be designed in compact form so that production units can be arranged side by side in a manufacturing area. Assuming the sheet dimensions and transport rate given above (10 cm wide and 2.5 cm/min), 5000 such furnaces would be required to achieve $5 \times 10^6 m^2/yr$.

This research program began January 6, 1976. Its objective was to demonstrate the feasibility of the floating substrate sheet growth process for the growth of silicon. Since the epitaxial growth of silicon is well known and presents no problems, the current effort was focused on the nucleation and rapid growth of substrate silicon from supercooled melts. Studies were performed of:

1. supercooling
2. crystal growth from supercooled tin-silicon alloy
3. silicon uptake into tin from silanes
4. surface growth

The goals of this contract were the growth via this process of single-crystal silicon having 0.5 cm^2 area and the determination of the velocity of propagation of single-crystal silicon along a hot tin surface that has been supersaturated with silicon.

1. SUMMARY OF KEY RESULTS

Results obtained in the supercooling experiments were quite encouraging. Values of supercooling of tin-silicon melts as high as 78 °C and 39 °C were observed at 1100 °C and 1200 °C respectively. On the basis of recent work (see text) on the propagation of sheet dendrite, this implies a sheet propagation velocity of 0.5 cm/min at 1150 °C.

We have determined that silicon may be incorporated into tin melts by direct interaction with a flowing silane gas stream. Single-pass efficiencies greater than 30%, corresponding to the deposition of solid silicon at 1.8 μm/min, were measured. It was determined that silicon is incorporated into liquid tin at the same rate that it is deposited upon silicon substrates and that the rate of incorporation is independent of the degree of melt saturation.

Tin melts have been driven into saturation by means of silicon input from silane and dichlorosilane. Silicon melt concentrations achieved by gas stream input were limited to the saturation value because of crystal growth nucleated by silicon deposited upon the tray walls.

The growth habit of crystals nucleated spontaneously at the tin-silicon alloy melt surface has been determined. The crystal growth observed is consistent with dendritic and web growth from (111) singly twinned triangular nuclei. Examples of planar surface growth of small (<0.1 mm), thin crystals from these twined surface seeds have been observed, demonstrating, in principle, the feasibility of the process.

Surface growth having growth velocity as high as 5 mm/min was obtained. This surface growth generally took the form of interlocking crystals and was thin enough to follow the liquid surface.

We were unable, however, to propagate large area single-crystal silicon growth along the surface of the tin-silicon melt. Small single-crystal regions often appeared but did not continue to propagate. They persisted for only a few millimeters and then reverted to branched dendritic growth.

The reasons for the polycrystalline growth are not clear. The most probable cause is the poisoning of the growth interface by impurities, either in solution or at the melt surface.

Section II

TECHNICAL DISCUSSION

1. SUPERCOOLING

a. TIN CLEANING AND PREPARATION

High-purity tin obtained from Kawecki Berylco Industries has been used in most of our experiments. This is obtained in the form of 1200 g billets and is designated 5N5 purity (99.9995 percent). The chemical analysis supplied by the vendor is tabulated below:

Chemical Analysis, ppm

Cu - 1.6
Fe - 0.09
Cl - 0.29
S - 0.81
Pb - 0.17
As - 0.02

Other elements are beyond detection.

Charges of the desired size were cut off with a saw and etched clean with a 1-1-1 etch, which consists of equal parts of HF, HNO_3, and H_2SO_4. This etch attacks tin fairly rapidly and yields a bright surface while in the etch. It must be quenched very quickly to prevent staining. Other etches that were examined were HCl and 1:1:4 HNO_3, acetic acid and glycerol. Concentrated HCl attacks Sn, but leaves a matte surface, whose texture is strongly orientation dependent. It probably does a good cleaning job, but, because of the textured surface which is produced, it is difficult to judge whether any stains have been left. The 1:1:4 etch also yielded a bright surface.

The etched tin billet was then melted under an atmosphere of H_2 or N_2 and poured through a capillary funnel into a casting mold to produce an ingot of the required form and weight, to fit into the supercooling apparatus. A properly cleaned melt will show no evidence of any dust of film when examined in a darkened room using a microscope lamp to illuminate its surface. The casting system is shown in Figure 2.

Quartz or pyrex make suitable molds except that the tin often sticks, causing them to break during cooling. Molds machined from extruded BN have been found to leave a faint film on the surface of the tin. Vacuum-fired graphite molds leave a film of graphite dust on the surface of the tin until they have been broken in by repeated use. They eventually clean up and yield ingots which

appear to be completely free of any surface contaminant. Pryolytic BN would probably have been even more suitable, but crucibles of the proper size were not available at the time that the supercooling experiments were performed.

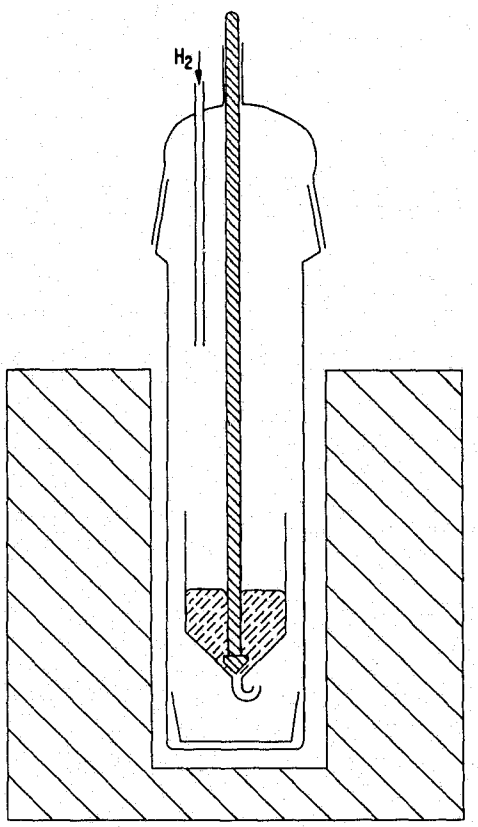

Figure 2. Tin Casting Apparatus

Samples which were produced by this procedure and cast in hydrogen directly into the crucible to be used in the supercooling experiment appeared to be completely free of surface contamination as judged by visual observation.

Upon melting in the supercooling apparatus, however, two kinds of surface contamination were evident. One, called "scum", formed a thin film covering part of the Sn surface and gathered into a small circular disc on the center of the melt under the gas jet as the melt was raised to 1200 °C.

The second form of contamination observed on the melt surface was called "fluff." It was only observed on melts that have been previously heated in the quartz crucible and are being reused. Upon reheating, a thin transparent film is observed to blister up from the surface of the Sn and then gather together into a very tenuous fluff ball, which is sometimes blown away by

the gas jet. The fluff is rapidly attacked by HF fumes and is presumably SiO_2 which has been dissolved from the crucible and forms on the surface of the melt as it is cooled to room temperature.

Auger analysis measurements were made on four of the tin ingots taken from the vertical furnace, in an attempt to determine the composition of the films and residues which form on the surface of the melts. Two samples were taken from KB-21 and KB-22, which had been melted in quartz crucibles with no Si added. The area where a small scum patch had gathered showed a strong carbon line, accompanied by weaker lines due to Sn, O, and Cl. Si was also seen at times. In KB-24 the Sn was melted in a BN crucible, and the scum from this sample showed both B and N to be present accompanied by C, Sn, and O at about the same intensity. KB-25 was likewise melted in BN, but had 2.5 wt percent Si added. This showed a similar spectrum. Si was not observed, indicating that the surface film was thick enough to eliminate the response from this element.

The Auger experiments show that carbon is a principal constituent of the scum which forms on melts prepared in quartz crucibles, confirming previous indications. As expected, BN is present on the surface of melts grown from BN crucibles. The Cl seen in the spectra from KB-21 and KB-22 may have come from using HCl in other experiments that were run using the same gas manifold. No lines due to foreign metals were observed. The carbon probably came from the graphite susceptor of the vertical furnace.

b. APPARATUS

A vertical furnace was used for the study of supercooling. It is shown in Figure 3.

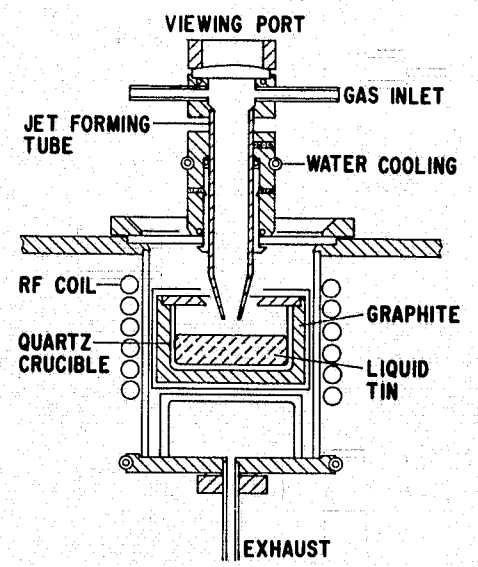

Figure 3. Apparatus for Supercooling Studies

The purpose of this equipment was to determine the supercooling that can be achieved in the absence of contact with a foreign surface. A crucible containing Sn-Si alloy was heated in an isothermal enclosure under a hydrogen atmosphere until all the silicon had dissolved. At this point, the temperature was measured, and an optical pyrometer reading was taken of the surface in order to determine the emissivity correction of the liquid. A jet of cold hydrogen was then directed upon the center of the alloy as indicated in Figure 3, to reduce the temperature of this portion of the liquid. The decrease in temperature was followed by means of optical pyrometer measurements and the value at which crystals began to form on the surface of the liquid indicated the amount of supercooling that was achieved.

c. CRUCIBLE MATERIALS

In conducting the supercooling experiments, we worked with crucibles made of fused quartz, BN, alumina, and graphite. BN and alumina appear most suitable as containers for the Sn-Si alloy.

Fused quartz is attacked to some extent by hot tin. When a pure tin charge is heated for the first time to 1200°C in quartz under a hydrogen atmosphere, the surface appears bright and clean except for a small patch of scum which generally gathers together and floats near the center of melt. However, if the tin is cooled and then reheated, one observes that a thin transparent film lifts off from the surface of the melt and gathers together into a tenuous "fluff ball." X-Ray and chemical analyses of the fluff have shown that it is SiO_2 with particles of metallic tin. This fluff formation occurs repeatedly each time the tin is cooled again and reheated in quartz but has not been observed when other crucible materials were used.

BN appeared quite promising for this purpose. Extruded BN contains considerable B_2O_3 and other impurities and results in considerable scum accumulation on the surface of the melt. On the other hand, pyrolytic BN ("Boralloy" crucibles obtained from Union Carbide Corporation) is much cleaner and appears to undergo little reaction with the melt. Furthermore, there is no adhesion between the crucible and its charge when the system is cooled to room temperature.

Morganite alumina crucibles also appear to be quite non-reactive and leave only a small amount of scum on the melt surface. They have the practical disadvantage of sticking firmly to the solidified charge after the system has been cooled.

Graphite behaves nicely with pure tin, but, when silicon is added, the melt wets the crucible and forms a firm bond upon cooling.

d. TEMPERATURE MEASUREMENT

We found it convenient to measure the temperature of the Sn-Si alloy by optical pyrometer measurements of the free surface of the liquid alloy. In order to obtain the proper temperatures, we had to determine the emissivity of the alloy melt.

In Experiment 59-5, we added 1.5 weight percent Si to a previously melted Sn charge weighing 124 g, in order to produce a saturated melt at 1100 °C. Temperatures were determined by means of an optical pyrometer which viewed the free surface of the melt at normal incidence and therefore did not "see" radiation from other parts of the furnace. At the dissolution temperature the pyrometer read T_{Sn} = 1015 °C, and a reading taken on some remaining Si showed an apparent temperature difference of 55 °C. Since the emissivity of Si has been measured (F.G. Allen, J. Appl. Phys, 28, 1510 (1957)) to be 0.55 in the temperature range 1100 to 1200 °C, these results yield a calculated value of 0.28 for the emissivity of the liquid Sn-Si alloy. We were unable to find any published reports giving the emissivity of liquid Sn with which to compare this result. Additional measurements of this kind confirmed this result; that the spectral emissivity of the alloy melt at 0.65 μm is 0.28 over the temperature range 1100 to 1200 °C.

e. SUPERCOOLING RESULTS

A series of supercooling experiments was performed with Kawecki tin. Several kinds of crucibles were used as described above, and tests were conducted using Si/Sn weight ratios chosen to give saturation temperatures near 1100 to 1200 °C, respectively. The values of supercooling measured during these experiments are plotted in Figure 4. Point "6-9" represents the average obtained using different positions of the cooling gas jet and flow velocities. More supercooling was obtained with large flow rates and with the jet close to the surface of the liquid. After run 17 was completed, the charge was removed for examination and then replaced and rerun with the upper heat shield removed to give "17 Remelted."

There is considerable scatter among the various ΔT values, much of which can be attributed to the use of different gas flow rates and H_2/N_2 ratios, as well as to different positions of the inlet tube. Nevertheless, a clear trend toward less supercooling is evident with increasing silicon content. This trend is consistent with observations reported in other alloy systems.

The supercooling results that we have obtained have been the result of nucleation by the scum floating on the surface of the melt. Greater supercooling would presumably result if the scum were eliminated.

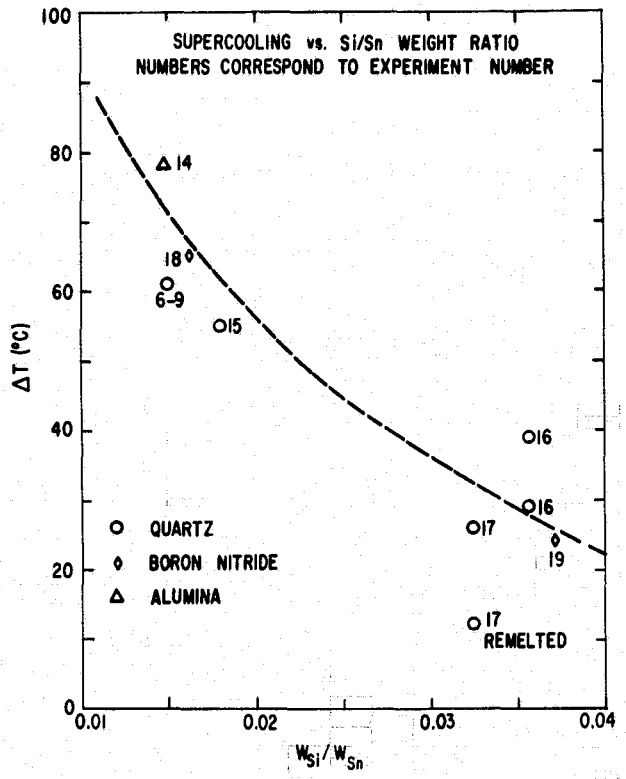

Figure 4. Supercooling vs Si/Sn Weight Ratio. The cluster of points near ratios of 0.016 corresponds to 1100 °C, and that near 0.035 corresponds to 1200 °C.

The usual measure of the degree of supercooling is the ratio $\Delta T/T_m$, where T_m is the melting point in degrees K. In the above experiment we have obtained $\Delta T/T_m=0.02$ at 1200 °C and 0.05 at 1100 °C. These values are much smaller than those obtained under conditions of homogeneous nucleation.

When supercooling is determined by homogeneous nucleation, this ratio is found to be in the range 0.13 to 0.26 for various pure metals [A.G. Walton, p.225 in "Nucleation" ed. A.C. Zettlemoyer, Marcel Dekker (1969)] and somewhat less for supercooling of liquid metal alloys [D.H. Rasmussen and C.R. Loper, Acta Met. 23, 1215 (1975)]. These values were determined by using emulsions of tiny droplets of the metal under study.

Recent publications by Trivedi et. al.* provide a basis for estimating the growth parameters that might be expected for the propagation of a sheet dendrite through a supersaturated tin solution. The growth velocity can be put in the form:

$$v = \frac{27D\Omega^3}{256\pi r_c}$$

*R. Trivedi, Metallurgical Trans, 1, 921 (1970); W.P. Buszo & R. Trivedi, Metallurgical Trans, 5, 511 (1974).

where Ω is the supersaturation parameter and r_c is the critical radius for nucleation. This formula must be regarded as crude because of the numerous approximations that were made. In particular, the introduction of r_c indicates that the result is insensitive to structural details that must be expected to play an important role in determining the rate at which new atomic layers are nucleated. The supersaturation parameter, Ω, is defined by

$$\Omega = \frac{C_\infty - C_o}{C_p - C_o} \quad ;$$

where C_o is the equilibrium concentration of silicon along the liquidus, C_∞ is the silicon concentration in the supersaturated condition, and C_p is the silicon concentration in the condensed phase. The value of C_p is 1 since this phase is substantially pure silicon. The Si/S_n weight ratio used in Figure 4 may be converted to the atom fraction Si, which is C_o. This corresponds to point B in Figure 1a and gives the temperature of the system. Under growth conditions the liquid is supercooled by an amount ΔT given by the separation between points A and C of Figure 1a where the silicon concentration is C_∞.

The data of Figure 4 may be used as described above to obtain values of the supersaturation parameter to be used in the equation above. The results are 0.025, 0.032 and 0.053 at 1050 °C, 1100 °C and 1150 °C respectively. Assuming $r_c=10^{-7}$cm (B. Chalmers, Principles of Solidification, John Wiley and Sons, New York, NY 1964) velocities of 0.03 cm/min, 0.07 cm/min and 0.5 cm/min are obtained for 1050 °C, 1100 °C and 1150 °C. These results were encouraging in that they indicated that reasonable growth rates might be anticipated in the temperature range above approximately 1100 °C, even with melts whose surfaces were not completely clean.

2. SILICON UPTAKE INTO TIN

a. APPARATUS

The gas control panel used for the experimental program is shown in Figure 5. It is designed to provide any mixture of the gases H_2, HCl, SiH_4, and SiH_2Cl_2 to an "active" reactor while maintaining a nitrogen purge flow in a second inactive reactor. The interchange between active and inactive reactors is conveniently accomplished by valving. This was done so two separate reactors, the vertical apparatus for the study of supercooling and a horizontal apparatus for the determination of silicon uptake from silane, can be serviced without the need for any replumbing. The gas control panel was leak-tested very carefully.

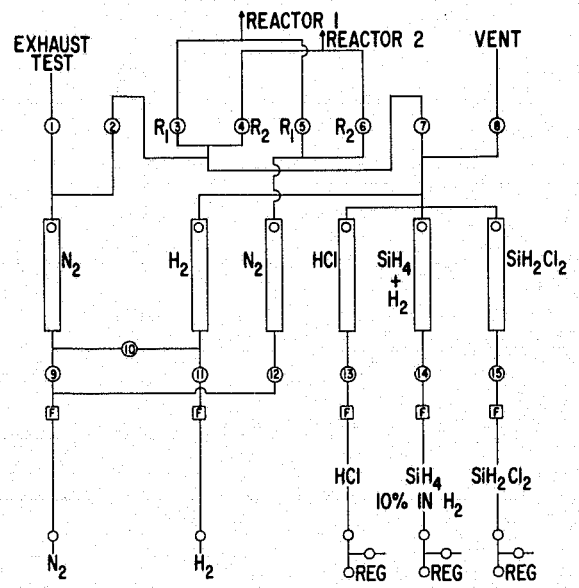

Figure 5. Gas Handling Panel

The apparatus of Figure 2 required that the initial tin billet be cut into pieces of the size required for each uptake experiment. This was wasteful and likely to introduce contamination. A second casting system was designed and built, which permitted the entire billet to be melted and poured as needed. This apparatus is shown in Figure 6. The Sn charge was melted in the outer chamber, and the amount needed was forced by N_2 pressure through a small nozzle into a graphite cup, where the Sn was allowed to solidify under a clean N_2 atmosphere. This procedure yielded Sn charges which were free of any visible surface film.

We had already determined in work performed prior to the current contract effort that silicon is taken up by liquid tin from an impinging silane gas stream. These experiments were extended in a systematic way to determine the rates of silicon uptake as a function of the solute and gas stream concentrations,

the degree of supersaturation that may be achieved, and whether it is limited by the formation of silicon nucleii at the surface of the alloy. This information is basic to determining the balance between two methods of supplying silicon to the growing edge of the silicon sheet: either directly from the incoming gas stream or by means of mass flow of alloy from a region where it had been brought to saturation at a higher temperature.

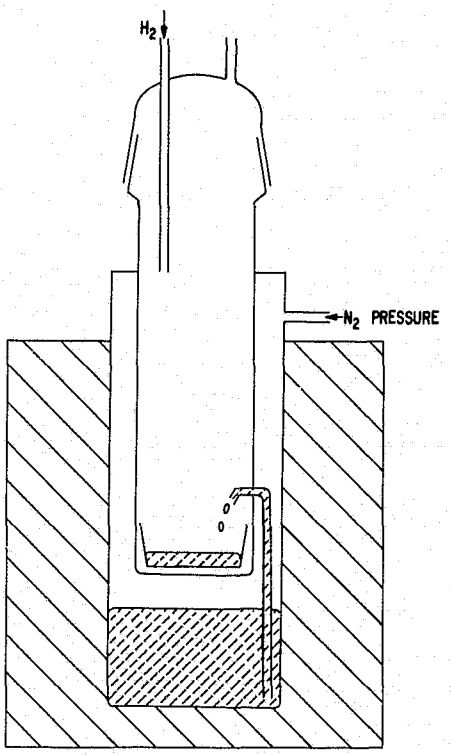

Figure 6. Improved Tin Casting Apparatus

The apparatus used in these experiments is shown schematically in Figure 7. It consists of a shallow horizontal quartz tray containing the tin charge, which is in thermal contact with an RF heated graphite susceptor. The reactor is water-cooled to prevent Si depletion from the incoming silane-bearing gas stream and to prevent Si from being deposited upon the inner surface of the quartz tube. The temperature is determined by means of optical pyrometer measurements of the surface of the tin melt and of the susceptor. The gas stream is designed for "forced laminar flow" so that there is a well-defined gas velocity and interaction length.

The experimental procedure was to heat the charge to a fixed temperature, expose it to the H_2/silane mixture for a fixed time, quench to room temperature, and weigh it. The incorporation of Si from the gas into the liquid is given directly by the change in weight - the loss of tin being negligible at the temperatures of interest, as will be shown below.

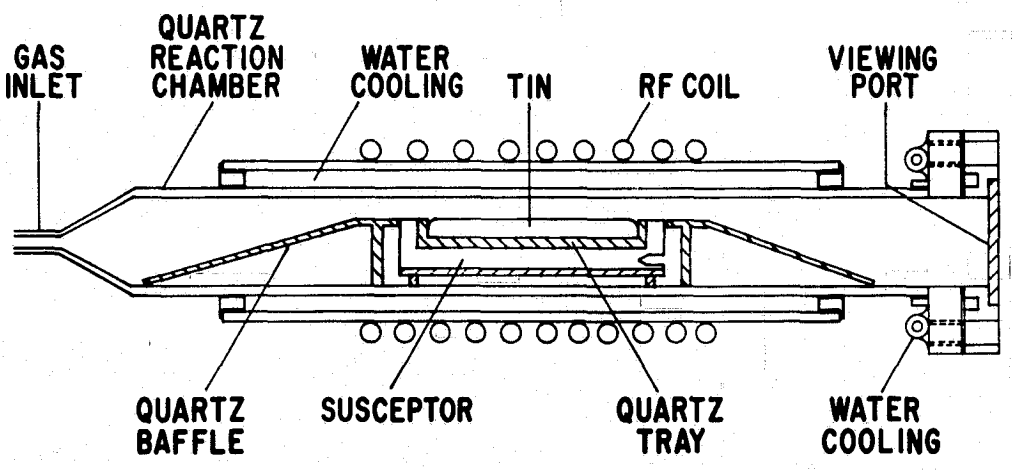

Figure 7. Horizontal Reactor

b. HOMOGENEOUS NUCLEATION

Two series of experiments, designated H8 and H9, were performed to determine the flow rates of HCl necessary to suppress homogeneous gas phase decomposition of SiH_4. The apparatus used was the horizontal system described above. Gas mixtures of H_2, N_2, SiH_4 and HCl were passed over a heated graphite susceptor. The temperature was measured with an optical pyrometer. The sightings were taken into a hole drilled into the graphite, so no emissivity corrections were required.

The presence of gas phase decomposition of the incoming SiH_4 was determined visually. The region above the susceptor was illuminated by an intense beam of light incident from above. Solid silicon particles in the gas stream were easily seen by the light that they scattered out of this beam. Our procedure was to set the desired flows of H_2, N_2, and SiH_4 with the HCl flow initially at zero. Under these conditions, with exceptions to be discussed below, silicon "smoke" was formed in the gas stream. The flow of HCl was then increased until the formation of this "smoke" was totally suppressed. The HCl flow rate was cycled through this value several times in order to verify the result.

When homogeneous nucleation occurred, silicon particles were observed in a narrow band less than one millimeter wide located approximately five millimeters above the hot graphite surface. This band of "smoke" was planar, indicating that the gas flow in the hot zone was laminar. High sensitivity in the detection of the onset of homogeneous gas phase nucleation was achieved by sighting along this plane. HCl flow rates were determined to a precision of 5 cc/min, and the SiH_4 rates are accurate to 0.7 cc/min. All flow meters used were individually calibrated against a Brooks Model 1055 Gas Flow Calibrator.

Measurements were made at 1015 °C and at 1135 °C for hydrogen flows of 900 cc/min and 2000 cc/min. Two concentrations were run, since hydrogen was expected to inhibit the decomposition of silane via the reaction

$$2H_2 + Si \rightarrow SiH_4 \quad .$$

The flow of N_2 was in all cases kept constant at 1200 cc/min.

For each set of experimental conditions there was a threshold SiH_4 flow rate below which there was no homogeneous nucleation even without any HCl. These were 14.7 cc/min and 33.5 cc/min for the low and high H_2 flow rates at 1015 °C, and 4.2 cc/min and 11.6 cc/min at 1135 °C. The results obtained are presented in Figure 8.

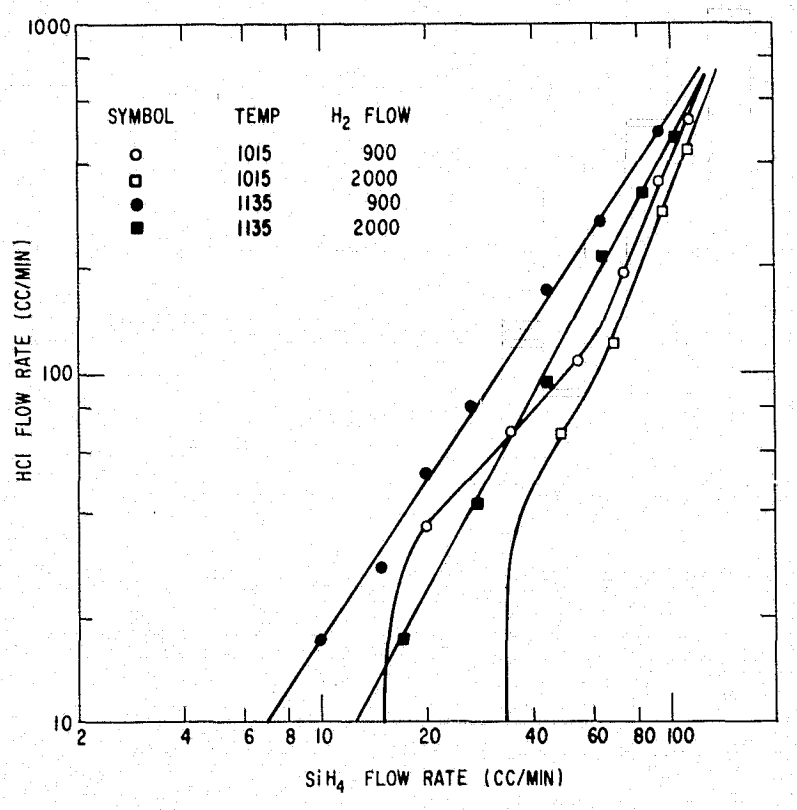

Figure 8. Boundary Lines for Homogeneous Gas Phase Nucleation of Silicon Growth from Silane

Each curve marks the boundary separating the regime of homogeneous gas phase decomposition from that where essentially all the silicon that is extracted from the gas stream is deposited upon the hot susceptor. The region generally above and to the left of these curves represents the gas flow conditions under which silicon uptake experiments may be meaningfully performed.

The reactor used for these experiments had internal dimensions of 2.5 cm x 5.7 cm. An additional series of experiments was performed in a second, larger, horizontal reactor. It has internal dimensions 3.5 cm x 6.2 cm, allowing a height of 1.4 cm for gas flow above the susceptor-tray assembly. This is twice the height available in the previous smaller reactor, permitting much better viewing of the tray contents from the end port.

The onset of homogeneous gas phase nucleation of silane decomposition was determined for this larger reactor following the procedure described above. The results were similar to those previously obtained and are shown in Figures 9 and 10. As before, there is a threshold SiH_4 flow for each set of conditions below which gas phase nucleation is absent. Beyond this, increasing amounts of HCl are required to prevent silicon formation in the gas stream. Increasing amounts of hydrogen suppress the formation of silicon, as before. These results differ somewhat in detail from those previously obtained in that (1) the present threshold SiH_4 values are somewhat lower than the corresponding previous ones (probably due to decreased cooling from the cold reactor wall which is twice as far away as previously), and (2) the amount of HCl needed at high SiH_4 rates is somewhat smaller. An especially noteworthy feature of the results shown in Figure 9 is the marked decrease in silane concentration associated with the addition of N_2 to the gas stream. Nitrogen is chemically inert at 1000 °C so this result must be due to the decrease in the thermal conductivity of the gas.

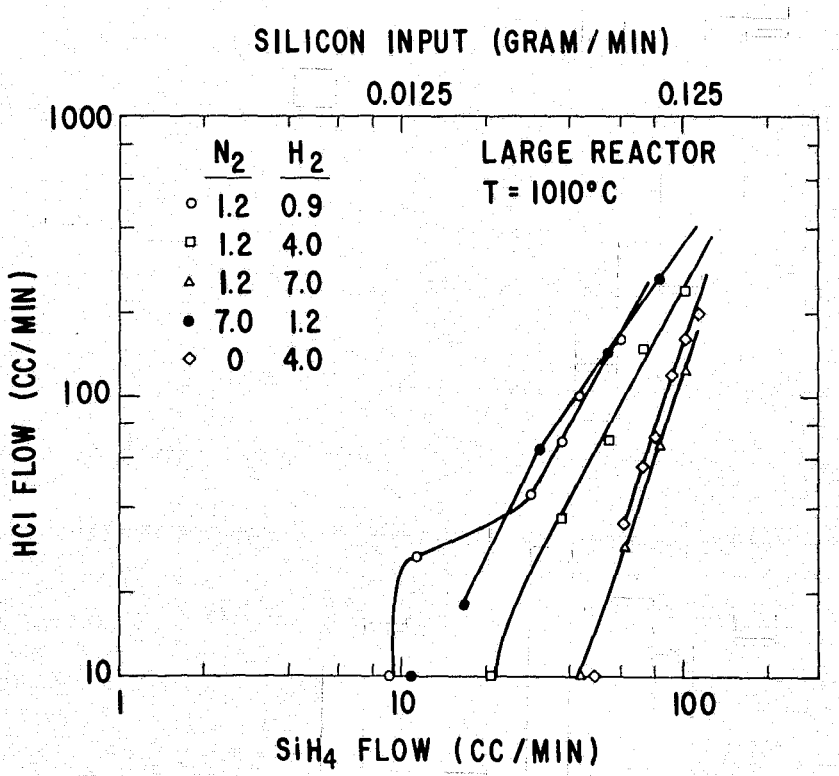

Figure 9. Onset of Homogeneous Nucleation in Large Reactor at 1010°C. (H_2 and N_2 Flow Rates in l/min.)

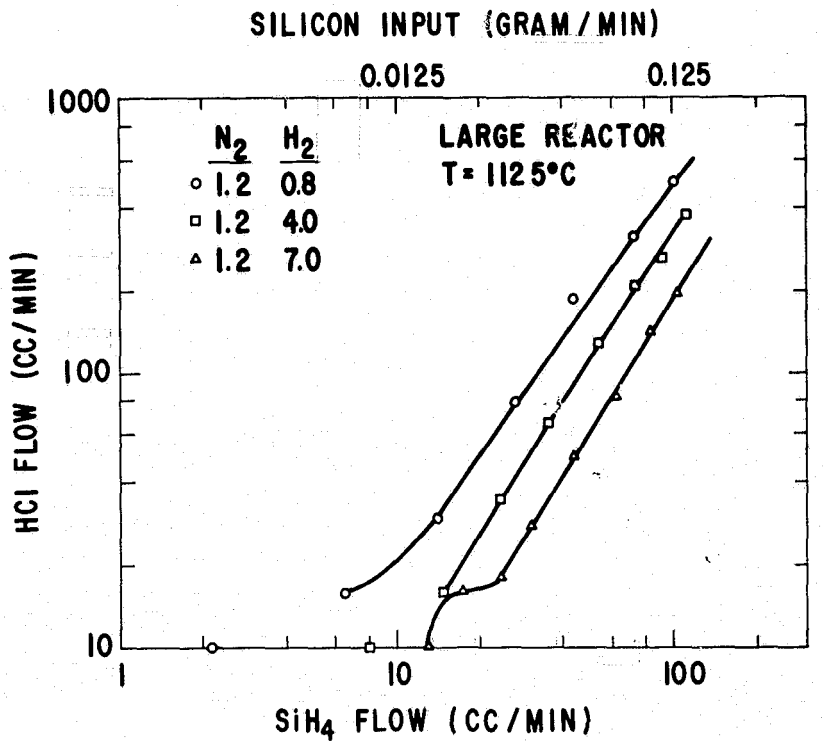

Figure 10. Onset of Homogeneous Nucleation in Large Reactor at 1125 °C. (H_2 and N_2 Flow Rates in l/min.)

c. SILICON DEPOSITION

Several preliminary experiments were performed in the small and the large reactors to measure the conversion of SiH_4 to silicon. These are listed in Tables I and II.

Table I

Preliminary Silane Conversion Experiments in Small Reactor

RUN #	T (°C)	SiH_4 (cc/min)	HCl (cc/min)	Time (min)	Substrate	δW (g)	f
H4S	1040	7.9	0	21	Sn	0.045	0.21
H6S	1050	27.3	45	57	Silicon Wafer	0.623	0.32
H7S	1040	10.7	0	63	Sn	0.189	0.22

Table II

Preliminary Silane Conversion Experiments in Large Reactor

RUN #	T (°C)	H_2 ℓ/min	SiH_4 cc/min	time min	δ W gm.	f	COMMENTS
H29L	1010	7.4	40	30	.226	.140	
H30L	1010	4.2	20	30	--	--	Tin splashed from tray
H31L	1010	7.5	53.5	30	.282	.175	Mo tray
H34L	1025	2.2	20	40	--	--	Tin splashed from tray

The substrate for Runs H4 and H7 was a pool of molten tin held in a rectangular quartz tray 3.2 cm wide by 6.4 cm long. The substrate in run H6 consisted of 2 silicon wafers presenting an area of 30 cm^2 to the gas stream. In addition to the SiH_4 and HCl flows shown in the table, hydrogen and nitrogen at 3.4 l/min and 1.2 l/min, respectively, flowed in the system in all cases.

A silicon sample was included as a substrate for several reasons: first, to act as a baseline sample to indicate whether the rate of reaction of SiH_4 at the liquid tin surface and the subsequent dissolution of the resultant silicon are grossly different than the corresponding reaction and deposition upon single-crystal silicon, and second, any variation in thickness of deposit in the direction of the gas flow may be used to study the depletion of SiH_4 from the gas stream. Finally, if the total rates of deposition on the liquid and solid are comparable, the spatial distribution of silicon deposited on the solid substrate, which is easily measured, indicates the variation of silicon uptake along the liquid tin surface. This cannot be measured directly due to rf stirring of the liquid.

The substrates were weighed to an accuracy of 10 μg at the outset of each run. They were then inserted into the reactor and the hydrogen and nitrogen gas streams were turned on. The temperature was next brought up to the value shown in Table I. After the temperature had stabilized, the indicated SiH_4 and HCl flows were added to the gas stream and were allowed to react with the substrates for the times shown. The active gases were then shut off and the system cooled to room temperature. The substrates were then reweighed. The weight change was in all cases positive and is given in the column marked δW of Table I. The SiH_4 and HCl concentration were such that homogeneous nucleation was suppressed. The ratio of the amount of silicon deposited upon the substrate (the weight gain) to the total amount of silicon that entered the reactor as SiH_4 during the run is given in the last column of Table I.

The liquid tin dissolved approximately 20 percent of the incoming silicon in both cases, although the total silane flux varied by a factor of four. This indicates that the uptake rate of silicon by the tin is linear up to the concentration represented by the 0.189 g of H7. The initial charge weighed 51.6 g, yielding 30% of saturation.

Thirty percent of the incoming silicon was deposited upon the silicon substrate (H6) compared with 20 percent for the tin. As was made clear by subsequent results, the reason for the difference was the geometry of the experiments. The tin substrate covered only 32 mm of the 57 mm width of the reactor, whereas the silicon substrates were 50 mm wide. The ratio of the two widths is 1.56, accounting for the difference.

Runs H30 and H34 provided no information because tin splashed out of the tray making it impossible to get a meaningful weight change. Useful data were obtained from runs H29 and H31 for which the measured uptake efficiencies were 14% and 18% respectively. The weight gains obtained after 30 minutes corresponded to 41% and 51% of saturation at the operating temperature of 1010 °C.

A molybdenum tray was used for run H31 to avoid cracking of the quartz trays and also in the anticipation that it would be wetted by the alloy melt. While the Mo did not crack, it was not wetted by the alloy melt.

The difference in conversion efficiency between the large and the small reactor is quite striking. It will be discussed below.

d. DEPOSITION ON SILICON SUBSTRATES

An extensive series of experiments was performed in the large horizontal reactor to measure the conversion of SiH_4 to silicon. H_2, N_2, SiH_4, and HCl flows were varied in order to establish overall trends and to determine the conditions for which the conversion to silicon was most efficient. Silicon wafers were used as substrates in order to facilitate the experiments and in order to allow a determination of the spatial variation of the silicon deposition. The temperature was held at 1010 °C. The general procedure was the weight gain measurement described above. In addition, the thickness of the deposit was measured. A tabular summary of these experiments is presented in Table III. The weight change δW, and f, the ratio of δW to the total amount of silicon entering the reactor as silane, are given in the last two columns of Table III.

The fraction of the incoming silane deposited as solid silicon is shown in Figure 11, where f is plotted versus hydrogen flow. Although f depends upon all of the gas flow rates, the data group themselves showing several well-defined trends. Curve A represents the simplest situation with no N_2 or HCl. There is a slow decrease in the efficiency of silane conversion

Table III

SILICON DEPOSITION EXPERIMENTS

RUN	H_2 ℓ/min	N_2 ℓ/min	SiH_4 cc/min	HCl cc/min	Time (min)	Total Gas Flow (cc/min)	δ W gram	f
H12	3.4	1.2	27.3	45	30	4900	.269	.261
H13	2.0	1.2	50	100	30	3700	.391	.206
H16	4.0	1.2	50	100	30	5775	.333	.178
H17	7.0	1.2	50	100	30	8775	.297	.157
H18	4.0	4.2	50	100	30	8775	.222	.118
H19	7.0	1.2	100	200	30	9300	.434	.115
H20	7.0	1.2	40	0	30	8600	.338	.224
H21	2	1.2	15	0	30	3350	.188	.332
H22	2	1.2	30	40	30	3540	.276	.244
H23	2	0	15	0	30	2150	.241	.425
H24	4	0	25	0	30	4250	.358	.380
H25	7	0	50	0	30	7500	.495	.239
H26	7	0	25	0	42	7250	.355	.269
H27	4	0	75	40	30	4790	.627	.258

from the high of 42% at 2.2 ℓ/min. of H_2 to 27% at 7.2 ℓ/min. Adding nitrogen to the gas stream decreases the efficiency. The addition of 1.2 ℓ/min of nitrogen, for example, takes one from curve A to the one marked B. The decrease of f with increased gas flow, either N_2 or H_2, is inconsistent with the stagnant layer model (F.C. Eversteyn et al., J. Electrochemical Soc. 170, 925 (1970)). The hydrogen effect that we observe may be due either to its suppression of the reaction $2H_2 + Si \rightarrow SiH_4$ or to a decrease in reactor dwell time caused by the increased gas flow. The nitrogen effect is almost certainly due to the decreased thermal conductivity of the gas.

The addition of HCl to the reactor gas stream, required at high silane concentrations, decreases f quite substantially. This is shown by curve C, which reproduces the H_2 and N_2 flow rates of curve B except for the addition of 100 cc/min of HCl. Further increases of N_2 or HCl continue to drive down the efficiency of silane deposition as is shown in Figure 11. The decrease in f with HCl concentration is caused by competing gas phase reactions which deplete the silicon by the formation of

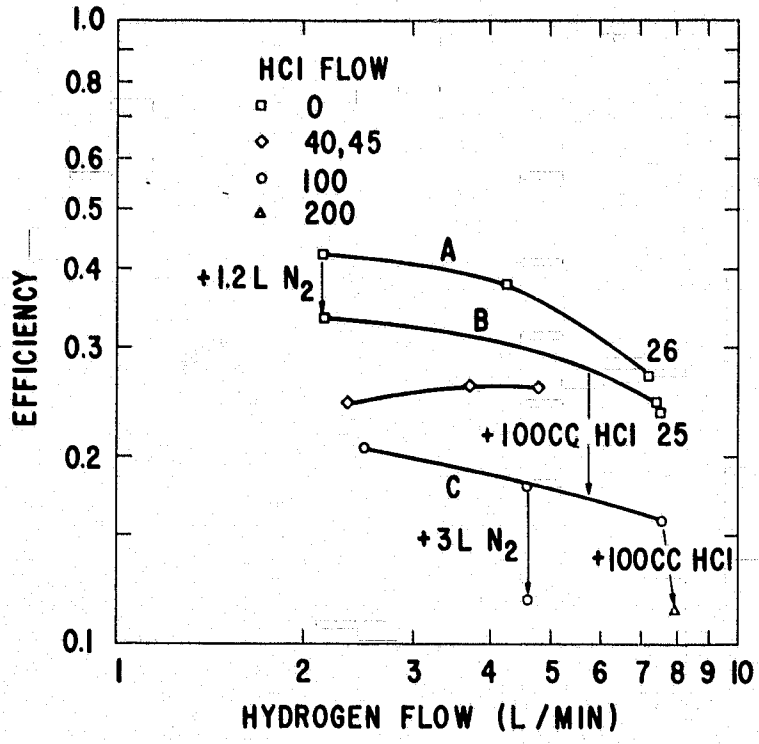

Figure 11. Efficiency of Deposition of Silicon from Silane upon Silicon Substrates at 1010 °C. Silane flow rates are listed in Table III.

polychlorosilanes of various types. We have seen both solid and liquid chlorosilane reaction products deposited upon the cold portions of the reactor. These substances are quite active, reacting slowly with atmospheric water and vigorously with liquid H_2O. Our experiments also show a dependence of f upon silane concentration, f decreasing slightly with increasing SiH_4. This is shown in Figure 11 by the data points labelled 25 and 26. As may be seen from Figure 11 and Table III increasing the SiH_4 flow from 25 cc/min to 50 cc/min, keeping all else fixed, dropped f from 0.269 to 0.239. The total deposit rate increased, of course, but not linearly with SiH_4 flow.

The Si depositions were in general, not uniform. They were usually heaviest toward the front of the susceptor, falling by 30% to 50% toward the end. At the highest gas flows, the silicon deposits were thickest somewhat downstream from the front of the deposition zone with diminished deposition at the front of the susceptor, because of the cooling effects of the incoming gas stream. Some typical examples of the spatial variation of the thickness of the silicon deposited is shown in Figure 12.

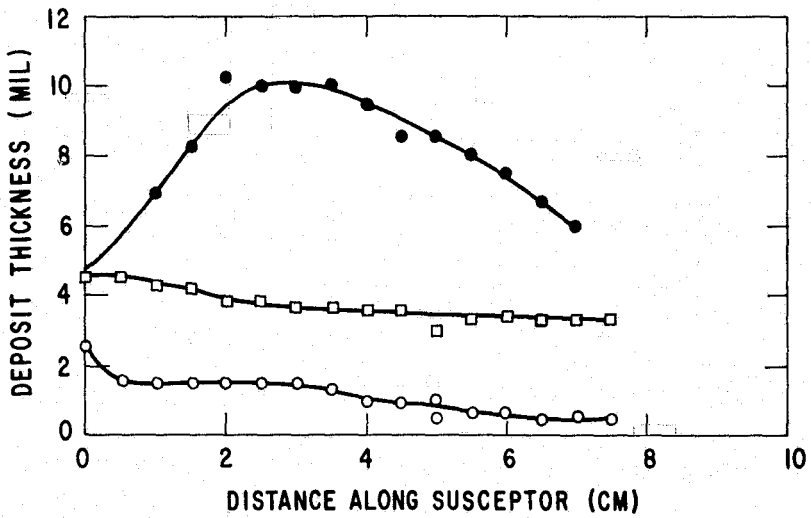

Figure 12. Example of the Variation of Deposition Thickness with Distance Along the Heated Gas Stream. (Silane concentration increases with increasing thickness of deposit.)

e. HYDRODYNAMIC INSTABILITY

We discovered an interesting hydrodynamic instability associated with tin melts. In the absence of any silane flow, the tin melt is stable, maintaining its position and configuration in the tray. With the addition of silane to the gas stream, however, the melt configuration is no longer stable. In the case where the melt does not cover the entire tray bottom, the liquid is observed to shift its position in the tray with a time constant varying from approximately 1 s to 100 s, depending upon silane flow rate. The motion is a sudden one, and droplets of tin are occasionally splashed out of the tray as the moving tin bounces off an end wall. When the tray is full, liquid motion also occurs. In this case the meniscus, which generally is concave down, suddenly flips up, the tin appearing to wet the wall along a small length. This small wetted length propagates about the periphery of the tray. The frequency of this motion is similar to that above. In this case tin may also be splashed out of the tray as the moving liquid hits a corner.

This phenomenon is based upon the fact that tin does not wet quartz. Although we have not measured the tin-quartz contact angle, it appears to be quite large. This, together with the large tin surface tension of 500 dyne/cm^2 at 1000 °C (B.C. Allen and W.D. Kingery, Trans. A.I.M.E. 215, 30 [1959]), leads to a large "head" of tin above the regions of the tray which are not covered. In the absence of any silicon deposition, this is a stable situation. With silane input, however, the situation is changed. At the same time as silicon is being incorporated directly as a solute into the liquid tin, it is also being deposited as a solid upon the hot portions of the tray which are not covered by the melt. There is a gap between this deposit

and the edge of the drop caused either by shadowing of the tray by the liquid edge and/or by surface diffusion of silicon along the quartz. When the solid film gets thick enough for the gap to be bridged at any point, the local contact angle suddenly becomes smaller, since silicon is wet by the tin alloy melt. The liquid now flows into this region of contact driven by its own hydrostatic head. It continues to flow until it is stopped by the walls, dissolving in the process all of the deposited solid silicon. No longer wetting the tray, the melt returns to its original area, reassuming something close to its initial configuration. This process continues as long as silicon is deposited upon the tray. The cyclic nature of the instability reflects the fact that the tray alternates between being wetted and not being wetted by the melt.

f. SILICON UPTAKE

A variety of experiments was performed in order to define an experimental configuration which would prevent the splashing of tin out of the tray. These are listed in Table IV. The small, 2.5 cm x 5.7 cm, internal dimensions reactor was used for these experiments.

Table IV

Run #	T	H_2 ℓ/min	SiH_4 cc/min	Tin min	δw gm	f	Comments
H37S	1015	4	27.4	30	.427	.42	Graphite boat
H38S	1000	4	20	65	.987	.61	continuation of H37
H39S	1010	4	21.5	60	.334	.211	.258 gm of solid silicon added at start
H40S	1015	4	35	36	—		excessive splashing flat susceptor
H41S	1005	4	20	45	.381	.34	flat susceptor curved ends
H42S	985	4	27.3	52	.277	.16	Mo
H43S	1002	2	20	32	.250	.31	tall tray, gas deflector for sides
H44S	1003	2	27.8	66	.677	.30	tall tray, flat suceptor

A graphite crucible was used in run H37 and in run H38, which is its extension. The tin charge was inserted directly into the graphite susceptor, which thus served also as the tray. The molten tin did not wet the graphite. Nevertheless, the tin motion was far less violent than previously observed due

to the ability of the alloy melt to wick along the irregular silicon-coated graphite surface once silicon had been deposited upon the walls by the decomposing silane. This wicking resulted in a layer of tin that "crept" up the walls, along the top, and partially down the sides along nearly the entire periphery of the susceptor/tray in the course of H37. This thin film of silicon-tin alloy which covers nearly all the surface of the tray not covered by the main body of the melt is a saturated film, since its local tin supply is quite limited. Upon continuation of this experiment in run H38 very heavy deposits of silicon developed upon the top walls of the tray, probably by the Vapor-Liquid-Solid growth process (R.S.W. Wagner and W.C. Ellis Trans. AIME 233, 1053 [1965]).

We abandoned further work with graphite upon these observations.

A Mo tray was used in Run H42. The Mo was cleaned prior to being filled with tin in order to remove any film which might have led to the nonwetting previously seen in run H31. The tray was thoroughly etched in a dilute 1:3 HF - HNO_3 etch and pre-fired to 1300 °C. The nonwetting and hydrodynamic instability persisted. It appears that Mo-Si is not formed at 1000 °C in the presence of tin. Further work with Mo was thus dropped.

A baseline experiment, H39, was run with our standard rectangular fused quartz tray. In addition to the tin charge of 54.06 g, a silicon wafer weighing 0.258 g was put in the tray in order to reduce the silane exposure needed for the melt to reach saturation. The experiment was run at 1010 °C for 60 min. The instability previously described was present in the small reactor. Considerable tin was splashed out of the interior of the tray, adhering to the tray top and to the exterior vertical tray walls where silicon had been deposited by the silane stream. The photograph presented in Figure 13 is a top view of the tray and contents of run H39. The tin on the tray top and adhering to the outside walls are clearly seen.

Although tin splashed out of the tray, none was lost, allowing a meaningful measurement of takeup efficiency. The result, $f = 0.21$, is the same as was obtained earlier in this apparatus in runs H4 and H7. The silicon introduced into the melts of H4 and H7 correspond to 6% and 35% of saturation, respectively, whereas H39 started out at 56% of the saturation value, indicating that the efficiency of silicon uptake is independent of degree of saturation.

In the next experiment, H40, the susceptor design was changed so that it was flat instead of completely surrounding the tray as before. In this manner we tried to inhibit the deposition of silicon on the tray walls by keeping them somewhat cooler than the melt. In addition, a gas deflector was introduced into the space above the tray so that essentially

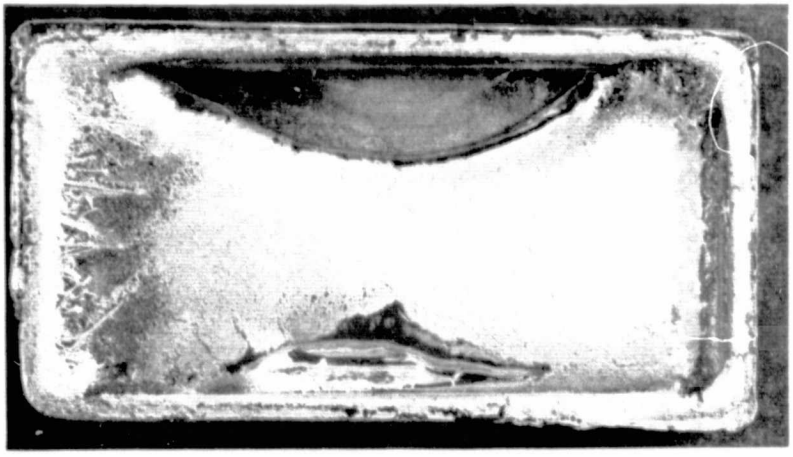

Figure 13. Top View of Run H39. Note the tin coated silicon deposit on the top of the tray walls.

all of the incident gas stream was forced to flow over the interior of the tray. This run was unsuccessful. Enough tin splashed from this run to make the weight changes meaningless.

We next used a tray which had an extra set of curved end walls inserted within the usual straight ends. The purpose here was twofold. First, we hoped that the motion of the tin would be deflected more gently by the curved walls than by the straight walls, and, second, that, if there were some splashing, the "spray" would be caught by that portion of the tray between the two walls which was initially unfilled. The gas deflector was used in this run. The results of this run, H41, are shown in Figure 14. There was splashing, but all the tin remained within the overall rectangular area, allowing a meaningful measurement of silicon uptake. The melt picked up 0.381 g of silicon in 45 min with an efficiency of 34%. This efficiency is greater than anything previously obtained with tin. It is substantially the same as was obtained in H6, where the deposition was made upon silicon substrates. The reason for this is that, by using the gas deflector, we have forced all of the incoming silane to flow over the tray and to interact with the hot tin bath.

Tray depth was increased from 6 mm to 9 mm for Run H43 in order to contain such splashes as occurred. In addition, the gas flow deflector was modified so that the side walls of the tray were shielded from direct contact with the gas stream in order to prevent the buildup of silicon upon the tops of the tray walls. We were quite successful. While mass motion of the tin in the tray was observed, indicating that there was deposition of silicon upon the inside vertical walls of the tray, the additional 3 mm height prevented any tin from splashing out. The extension of the gas flow deflector over the tray walls was similarly successful as may be seen in Figure 15. The tops of the side walls show only a very light transparent

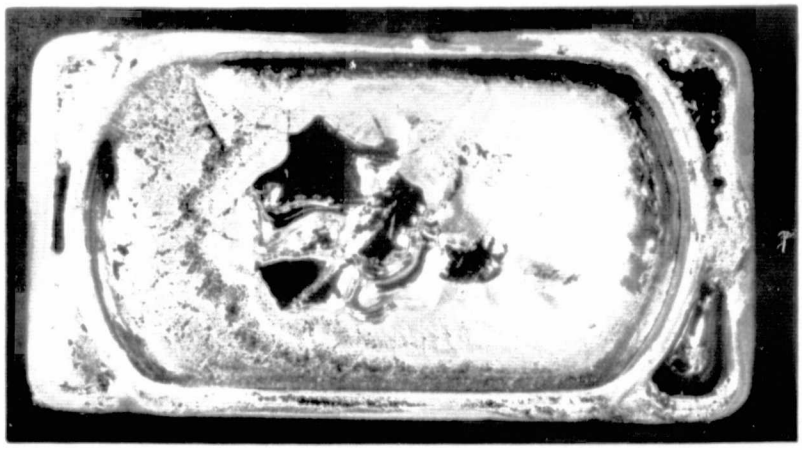

Figure 14. Top View of Run H41. The splashes were successfully caught and contained within the regions between the two sets of end walls which were initially empty.

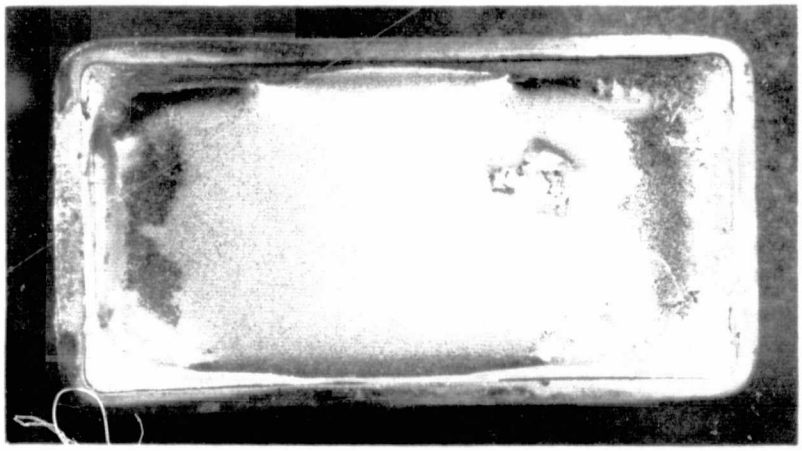

Figure 15. Top View of Run H43.

silicon deposit and show no trace of tin. The front and back which were left in the gas stream as controls show heavy silicon deposits. These were wetted by the tin which wicked up along the rough textured silicon deposit. In this run 0.250 g of silicon were taken up in 32 min at 31% efficiency.

The gas deflector was further modified to shield the front and back walls for Run H44. The tray walls were kept relatively cool through the use of the flat susceptor and by shielding them from direct susceptor radiation. These modifications resulted in essentially no deposition of silicon anywhere along the periphery of the tray top. The inner vertical tray walls, on the other hand, were coated, since silane was able to diffuse to them and the temperature was not low enough to prevent silane decomposition. The melt was, however, very quiet with no sign

of the hydrodynamic instability. As soon as the melt wet the walls, it clung to them, the tin being unable to dissolve all of the deposited silicon, fall away, and leave the wall clear for further silicon deposition. This was due to the reduced wall temperature, which, while not low enough to inhibit silane decomposition, was low enough to drastically reduce the local silicon solubility in the melt.

The silicon uptake was 0.677 g in 66 min with an efficiency of 30%.

Additional silicon uptake experiments were performed. They are summarized in Table V.

Run H46 was our initial effort at using boron nitride (BN) as the tray material in a silicon uptake experiment. The tray was machined from Union Carbide HBR grade material. It was soaked in methanol and prefired to 1300 °C prior to use in an attempt to eliminate the 4% oxide used as a binder. This treatment was insufficient. Examination of the tray after the run revealed small globules of a vitreous material adhering to the entire tray surface, including the part covered by the tin charge. Presumably the oxide is present as CaB_4O_7, whose melting point of 986 °C is below the run temperature of 1005 °C. Subsequent HBR BN trays, used in Runs H48 and H56 through H59, were fired in vacuum at 1680 °C for 4 hr to remove the tetraborate.

Table V

RUN #	T (°C)	H_2 (ℓ/min)	Si_4 (cc/min)	t (min)	δW g	f	COMMENTS
H46 L	1005	4	27.3	26	.140	.157	B.N. Crucible
H47 L	1020	4	27.3	137	-	-	Tin Splashed
H48 L	1000	4	23.6	31	.154	.160	B.N. Crucible
H48 L	995	4	23.6	102	.360	.123	Continuation of H48
H55 S	1050	4	27.3	34.5	.268	.369	Silicon Substrates in Tray
H56 S	1050	2	20	20	.180	.359	B.N. Crucible
H57 S	1040	2	20	15	.128	.341	Continuation of H56
H58 S	1050	2	20	15	.128	.341	Continuation of H57
H59 S	1050	2	20	15	.129	.340	Continuation of H58

These trays did not break upon cooling, thus allowing a sequence of experiments to be performed upon a single charge of tin. They also seemed to inhibit somewhat the mass motion associated with the hydrodynamic instability. They were not, however, as clean as the quartz trays. More scum was observed when they were used, especially in the case of H46.

Examination of the results given above for the uptake of silicon from silane reveals a consistent picture. The measured efficiencies fall into two groups: one associated with the small, 2.5 cm by 5.7 cm reactor, and the other obtained from the large reactor. Approximately 30 to 35% of the silicon in a silane stream passing over hot tin is taken into solution in the small reactor, whereas 15% is taken up in the large one. This difference is no doubt connected with the different geometry, especially the longer average gas diffusion distance in the bigger reactor.

Runs H56 through H59 are a sequence of silicon uptake experiments performed with a single tin charge. The melt started with no silicon content at the beginning of H56 and ended with 0.564 g of silicon corresponding to 70% of saturation at the conclusion of H59. There was no significant change in uptake efficiency through this sequence. This, coupled with the 31% observed for H43, which had the same geometry and which started at 88% of saturation, leads us to the conclusion that the efficiency of silicon uptake is independent of degree of melt saturation.

Run H55 had silicon wafers as substrates and had exactly the same gas flow geometry as the sequence H56 through H59. The wafers were placed in the bottom of the tray, covering 61% of its area. The silicon deposition efficiency for this run, normalized for area, was 37%. We conclude that the deposition rate of silicon from SiH_4 is independent of whether the substrate is solid silicon or liquid tin.

Several experiments were designed with the objective of bringing the Sn-Si alloy melt to saturation and beyond. Runs H43 and H44, for example, were begun with enough solid silicon added to the tray so that silane flows below the threshold of homogeneous gas phase nucleation could drive them to saturation in a short time. These experiments began at 88% of saturation. Runs H47 and H48 were simply run long enough for the melts to be saturated directly from the gas stream.

In none of these cases were we able to supersaturate the melt. Below saturation, the tray walls were kept clean by the mass motion and silicon dissolution associated with the hydrodynamic instability. The meniscus remained concave down under these circumstances. As the melt approached saturation, however, it was observed to attach itself to the tray wall along those regions where the "scum" happened to be. The meniscus in these regions was now turned up. With additional silicon input from the silane gas stream, crystals were observed growing in toward the melt from the tray wall. These crystals were nucleated by the solid silicon deposits on the tray wall which could no longer be dissolved by the melt because it was saturated. Silicon deposition on the tray walls thus prevented us from driving the Sn-Si melts beyond saturation.

g. USE OF DICHLOROSILANE

The deposition of silicon upon the inner tray walls by silane was the source of two serious problems: the hydrodynamic instability, and the initiation of undesirable crystal growth from the walls as the melt is brought to saturation by the gas stream. We conducted a series of experiments to determine whether the use of dichlorosilane would produce less silicon deposition on the walls.

Deposition upon silicon wafers was studied in Runs H49 through H53. The flat susceptor was used to minimize direct heating of the tray walls.

These experiments are summarized in Table VI.

Table VI

SILICON CONVERSION FROM DICHLOROSILANE

RUN #	T (°C)	H_2 (ℓ/min)	SiH_2Cl_2 (cc/min)	t (min)	δW g	f	COMMENTS
H49 L	1060	4	62.5	22	.0786	.072	Si substrate
H50 L	960	4	62.5	20	.0171	.016	Si substrate
H51 L	1190	4	62.5	20	.146	.145	Si substrate
H52 L	1100	4	62.5	21	.1065	.105	Si substrate
H53 L	1000	4	62.5	20	.036	.035	Si substrate
H54 L	1050	4	62.5	24	.136	>.072	Tin substrate

The wafers were placed on the bottom of a standard quartz tray to reproduce as nearly as possible the geometry with tin as the substrate. The work coil was adjusted so that the temperature of the tray bottom was uniform to better than 2 °C. Deposition rates were determined by measuring the weight gain of the wafers for given deposition time. Hydrogen was the major constituent of the gas stream at 4 ℓ/min and the dichlorosilane was kept at 62.5 cc/min.

The results obtained are shown in Figure 16. The data have all been normalized to the tray area of 20.5 cm^2. There is a marked variation with temperature. The rate increases with T up to the value 12 mg/min at 1200 °C -- corresponding to 15% conversion efficiency.

The tray sidewalls were not heavily coated. Only the bottom 3 mm or so accumulated any silicon--the top two-thirds remaining clean because of the rapid falloff of deposition on the relatively cool walls. This is shown in Figure 17.

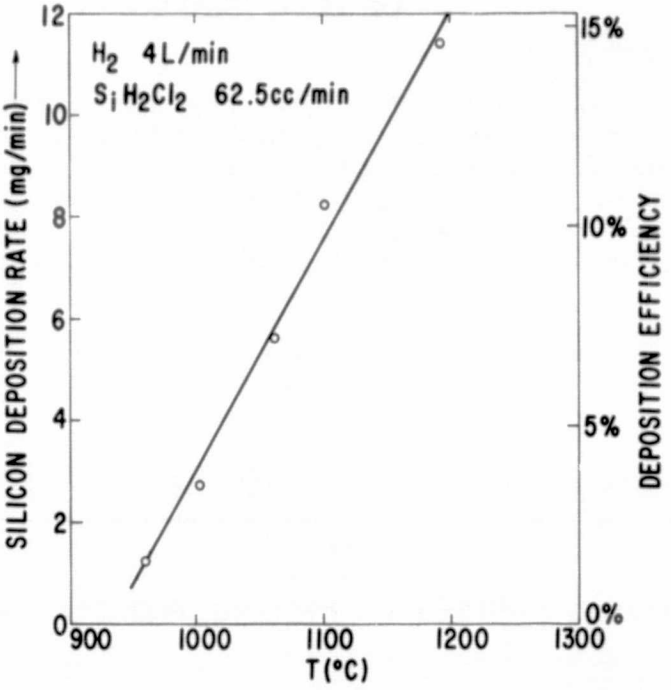

Figure 16. Temperature Variation of the Deposition Rate of Silicon From Dichlorosilane. Deposits were made upon silicon wafers 13 cm^2 in area

Figure 17. View of the Quartz Tray After H-51. The area covered by the silicon substrates and the silicon deposits partly up the walls are clearly visible

In Run H54, dichlorosilane was used as the silicon source and tin was the substrate. The flat susceptor was used, and the walls of the quartz tray were kept cool with quartz paper reflective insulation. The operating temperature of 1050 °C was chosen so that the tray walls, expected to be 100 to 200 °C

cooler than the melt, would not collect much silicon. Gas flows were the same as in the test runs using silicon wafers: 4 ℓ/min of H_2 and 62.5 cc/min of SiH_2Cl_2.

There was very little mass motion during this run, indicating that we had achieved a substantial reduction in the wall deposition rate. Nevertheless, after 15 min of dichlorosilane input, the melt, which hitherto had not wetted the quartz, was seen to adhere to the front wall of the tray. Subsequent examination showed that the tin-silicon alloy had wetted the front third of the tray and that silicon had been deposited in a band approximately 1 mm high along the entire length of the wetted region. This may be understood with the aid of Figure 18.

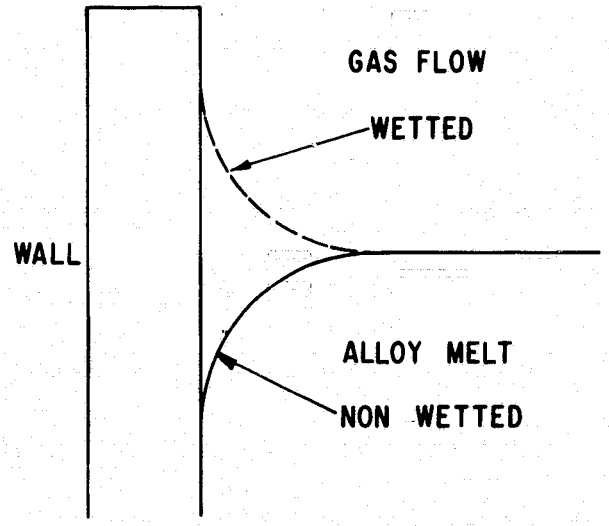

Figure 18. Schematic View of the Meniscus at the Tray Wall for the Wetted and Unwetted State.

In the initial, unwetted, state the upper section of the tray wall (above the horizontal plane of the melt) picks up silicon deposits quite slowly in spite of the fact that it has unrestricted access to the dichlorosilane gas stream. The reasons for this are the low temperature of this upper section resulting from the low thermal conductivity of quartz and the rapid decrease in the deposition of silicon from dichlorosilane as the temperature falls below 1000 °C. Silicon deposition upon the hot lower section of the tray is similarly light as a result of the limited solid angle that it subtends with the gas stream. With the melt well below saturation, this relatively light silicon deposition is quickly absorbed by the liquid. The walls remain clean, they are not wetted, the upper section remains relatively cool, and the low deposition rate is maintained. As saturation of the melt is approached, dissolution of the wall deposits proceeds more slowly. At the point at

which the deposition rate exceeds the dissolution rate, the melt begins to wet the tray wall. The miniscus flips up and the wetted portion of the tray wall immediately adjacent the tin-quartz interface now has unrestricted access to the dichlorosilane. The deposition rate increases substantially in a narrow band along this interface because the tray wall in this band is heated by direct conduction from the alloy melt. A thick silicon deposit is thus formed in a narrow band immediately above the edge of the wetted region.

Silicon crystals were observed to be growing out from the wall in the region where the melt was attached after a time that, on the basis of the silicon wafer data of Figure 16, should have been insufficient to saturate the melt. Subsequent weighing of the sample verified this, yielding a weight gain of 0.136 g consistent with the value of 0.127 g predicted by the data of Figure 16. Solid silicon weighing 0.466 g had been added to the tin charge at the outset of H54, making a total of 0.602 g of silicon in the melt--only 73% of the amount required for saturation at the operating temperature of 1050 °C.

There are several possible explanations for this apparently premature onset of saturation. There was some tin loss from the bath, since a white solid, presumably $SnCl_2$, was observed to deposit downstream of the tray upon the cool reactor walls. The measured weight gain is thus the net difference between the silicon gain and the tin loss, so the actual silicon uptake may have been considerably larger. The weight of silicon from dichlorosilane required to saturate the melt is 0.363 g, nearly three times the observed 0.136 g. Since the measured value is quite close to the number expected from the deposition data upon silicon, this explanation is unlikely. While there was some tin loss, it probably was not large. Additional work will be required to determine the rate of tin loss to the dichlorosilane.

Another possible explanation is nonuniform, heavier deposition of silicon toward the front of the tray. This is unlikely, since it was not seen in the experiments done with silicon wafers.

The most probable explanation is that the silicon crystals grew because the melt temperature along the wetted interface at the tray wall is lower than that of the main body of liquid. This region, therefore, becomes saturated well before the rest of the tin. The meniscus along the wetted periphery had climbed approximately 2 mm higher than the main melt surface, making it quite reasonable that the temperature at the melt-wall interface was at the 1005 °C required for local saturation.

h. STABILITY OF TIN MELTS

The rate of tin loss at 1010 °C to the gas stream was determined for hydrogen and also for the case where 100 cc/min of HCl was added to 2 ℓ/min of H_2 flow. In the case where only

H_2 was used, the 42 g charge of tin lost 0.5 mg in 30 min, corresponding to 4 x 10^{-5} percent loss per minute. At this rate 17.3 days would be required for the bath to lose 1% of its tin. When HCl was added, the loss was much greater. The 42 g charge lost 0.762 g in 20 min, for a rate of 0.09%/min. This rate is much too high for any practical reactor.

i. SUMMARY

We have established that silicon can be incorporated into tin with single-pass efficiency greater than 30% and that this rate is independent of the degree of melt saturation. Measured incorporation rates have been 0.42 mg/cm^2-min corresponding to deposition of solid silicon at 1.8 μm/min. It has been possible to drive tin melts to saturation directly from the vapor.

We have, however, been unsuccessful in achieving supersaturation of the alloy melt from silane because of the deposition of silicon upon the tray walls. This solid silicon provides nucleation sites. Gas curtains are needed to prevent this deposition.

Tin baths are quite stable in hydrogen, losing only 6x 10^{-2}%/day at 1010 °C. HCl has, however, proven to be unsuitable, since the addition of as little as 5% HCl to hydrogen increases the tin loss to 5%/hr.

3. GAS STUDIES

In the course of early attempts at seeded surface growth in the horizontal reactor we observed film formation upon the silicon seeds. It prevented the seed from being wetted by the melt except in a very limited number of areas, and it interfered with the proper seeding of the new silicon growth. The film may be seen as the matte appearance of the seed surface in Figure 19 and by the thin rim along the dissolved edges of the seed where it was "rolled back" by the melt.

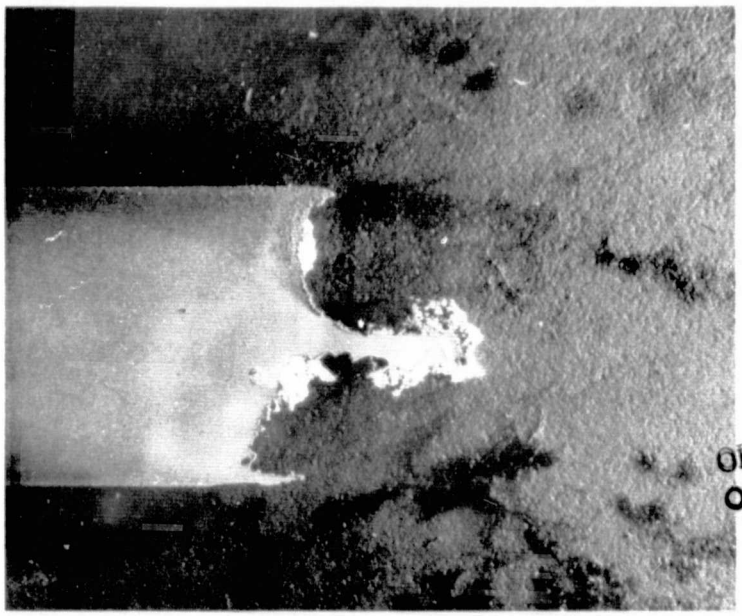

Figure 19. Surface Growth at a Silicon Seed Produced by Silane Flow in the Reactor. Film formation upon the seed was especially heavy in this instance, preventing growth except at the shiny areas.

We thereupon undertook a systematic study to isolate and identify the source of the films that had been developing upon our seeds. The means chosen was to use a clean, specular silicon surface as a detector. Any film formed, either by reaction of the silicon with oxidizing or carbiding impurities in the gas stream or by deposition in some other manner, was easily detected ellipsometrically. Chem-mechanically polished <111> silicon wafers were placed directly upon the graphite susceptor in the horizontal reactor. The wafers were dipped into 10% HF, rinsed, and pulled dry from deionized water just prior to being loaded into the reactor. Wafers were run at approximately 1100 °C under various gas flow conditions for about one hour. Specific gas flows, reaction times, temperatures, and brief summaries of the results are given in Table VII.

TABLE VII

Gas Studies

Run No.	H_2 (ℓ/min)	N_2 (ℓ/min)	T (°C)	t (min)	Thickness (Å)	Surface	Comments
G1	0	2	1150	60	34		Old endpiece
G2	0	2	1165	67	140		New endpiece
G3	0	4.4	1165	60	30-110	Smooth	
G4	2	2	1120	60	80-480		"Bulls-eye" pattern
G5	2	2	1120	60			
G6	0	4	1120	47	40		Uniform film
G7	3	0	1080	60	7	Pitted	
G8	2	2	1090	40	28	Smooth	Uniform film

Run G1 was made using the furnace endpiece which has no seals other than its static O-ring seal to the reactor. Under the conditions shown, with only nitrogen flow, a smooth 34 Å thick film grew upon the sample. This film proved to dissolve very slowly in 10% HF; one minute of etching removing only 7 Å. It cannot, therefore, be SiO_2. It is probably a silicon nitride film, although silicon carbide cannot be ruled out.

We used a more complex furnace endpiece for the next several experiments to determine whether the extra seals needed for the auxiliary gas flow and for the seed holder leaked. In addition, in Runs G3 through G8 we used the auxiliary gas flow as a means for allowing a jet of the gas to impinge directly upon the heated sample. Two samples were used in these runs, one of which was right in the jet flow.

While these results were not completely self-consistent (note the variation in the film thicknesses grown in Runs G2, G3, and G6), several results stood out quite clearly. First, the use of nitrogen produces a smooth film that is not SiO_2. Second, samples heated in hydrogen come out of the reactor very clean. While the surfaces exhibit etch pitting caused by thermal etching, especially in regions of high gas flow near the jet, the measured film thickness of 7 Å is about as small a value as can be measured under ordinary laboratory conditions. It is easily accounted for by two monolayers of oxide and/or water adsorbed upon the surface after removal from the reactor.

The results obtained with mixed hydrogen and nitrogen flow were puzzling. In Runs G4 and G5 the films on the samples in the jet flow grew in a "bulls-eye" pattern whose center is the jet axis. This may be seen in Figure 20. The thickness of the "bulls-eye" films varies from approximately 100 Å to 500 Å for G4 and slightly less for G5. The films upon the other wafers not in the jet flow were much more uniform in thickness: 80 Å to 90 Å for G4, and 35 Å to 40 Å for G5. The results for G4 and G5 agree

quite closely. However, the films obtained in Run G8 were very different in spite of the fact that the operating conditions for this run were nominally the same as those of G4 and G5. The well-developed bulls-eye pattern seen earlier was almost completely gone, and the films were fairly uniform at approximately 30 Å.

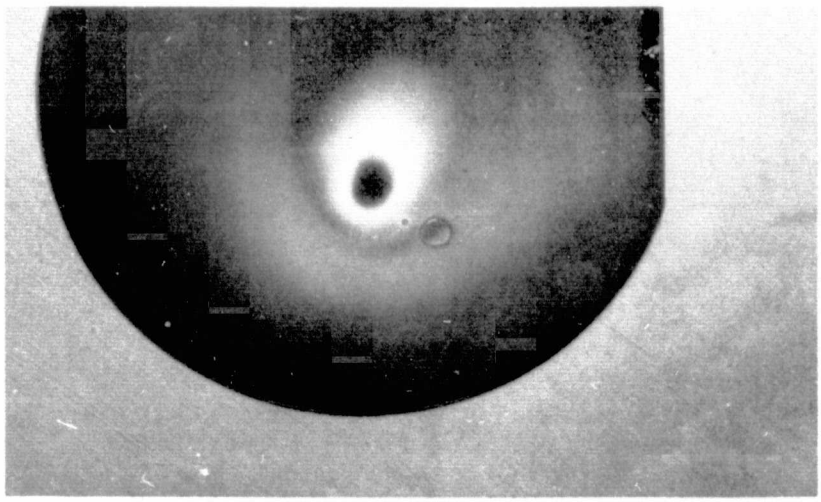

Figure 20. "Bulls-eye" Pattern Obtained in Run G5.

The qualitative difference between the films of G5 and G8 and the less striking, but nonetheless real, thickness differences in the films resulting from Runs G2, G3, and G6 - all run under nominally the same operating conditions - indicated that some important parameter was not under control.

There appeared to be a pattern in this variability: films obtained from later runs seemed generally to be somewhat thinner than those obtained in earlier experiments.

All of these experiments were performed with a graphite susceptor and interleaved quartz paper/molybdenum foil reflective insulation. Both of these were possible sources of variability and contamination, since they can absorb considerable quantities of air and water vapor upon exposure to the atmosphere, and release these gases with subsequent heating.

Additional experiments were performed. These are summarized in Table VIII.

TABLE VIII

Further Gas Studies

Run No.	H_2 ℓ/min	N_2 ℓ/min	T °C	t min	Thickness Å	Surface	Comments
G11	2	0	1100	45	6.5	slight etching	Si-coated graphite susceptor
G12	0	2	1095	45	26	smooth	Si-coated graphite susceptor
G13	2	0	1085	40	6	thermal etch	Graphite susceptor
G14	0	2	1085	50	28	thermal etch	
G15	2	0	1075	43	4	thermal etch	New endplate
G16	2	0	1075	45	4	thermal etch	Heavy etching under jet
G17	0	2	1075	55	30-130	smooth	
G18	2	2	1075	45	30-150	smooth	
V2-1	10	0	1075	40	-	severe thermal etching	Experiment performed in epitaxial reactor
V2-2	0	3	1075	45	35	smooth	Experiment performed in epitaxial reactor
V2-3	0	3	1200	32	53	smooth	Experiment performed in epitaxial reactor
V2-4	0	3	1075	123	49	smooth	Experiment performed in epitaxial reactor

The role of the insulation was tested in Runs G11 and G12. The quartz paper was removed for these experiments, leaving only molybdenum foil reflective insulation. The surface of the graphite susceptor was also sealed with a silicon coating. In a further attempt to carry out these experiments in as clean a configuration as possible, the endplate with a single static seal was used. The film obtained from G11, which was run in hydrogen, was 6.5 Å. The surface also exhibited mild thermal etching. These results are essentially the same as those obtained earlier with hydrogen: the surface was very clean.

Run G12 which was operated in nitrogen generated a smooth film 26 Å thick. While similar to the films seen earlier for nitrogen gas flow, it is somewhat thinner than the 34 Å and 40 Å obtained for G1 and G2, respectively.

Runs G13 and G14 are repeats of G11 and G12, using an uncoated graphite susceptor. This susceptor was made from Union Carbide high-density graphite and was fired in vacuum at 1700 °C prior to being used. The results obtained were identical with those from the sealed susceptor. We thus conclude that (1) the quartz paper was indeed the source of our variability, and (2) hydrogen-graphite reactions to form hydrocarbons with attendant contamination of the gas stream is not a problem.

The high-density graphite susceptor was used in subsequent experiments G15-G18. The furnace endpiece with the auxiliary gas

jet and additional sliding O-ring seals was used in order to determine the effect of the gas jet directed at the sample surface and to check whether these seals leaked.

G15 and G16 were performed with a pure hydrogen jet directed at a portion of the sample surface. The results were the same as those obtained earlier. Away from the jet, where the gas flow was relatively slow, the sample surface was smooth, allowing ellipsometer measurements. The surfaces came out of the reactor very clean, exhibiting 4Å-7Å films when measured within a minute or less or exposure to air. The regions of the samples near the jet where the hydrogen flowed along the surface at high velocity developed a pronounced thermal etch pattern as a result of the fact that the silicon evaporated from the clean surface is carried off by the gas stream. This pattern, which is centered about the jet flow, may be seen in Figure 21, an overall view of sample G16. Figure 22 is a microphotograph of the "hazy" region of G16. The thermally etched pattern with <111> crystal symmetry is clearly visible.

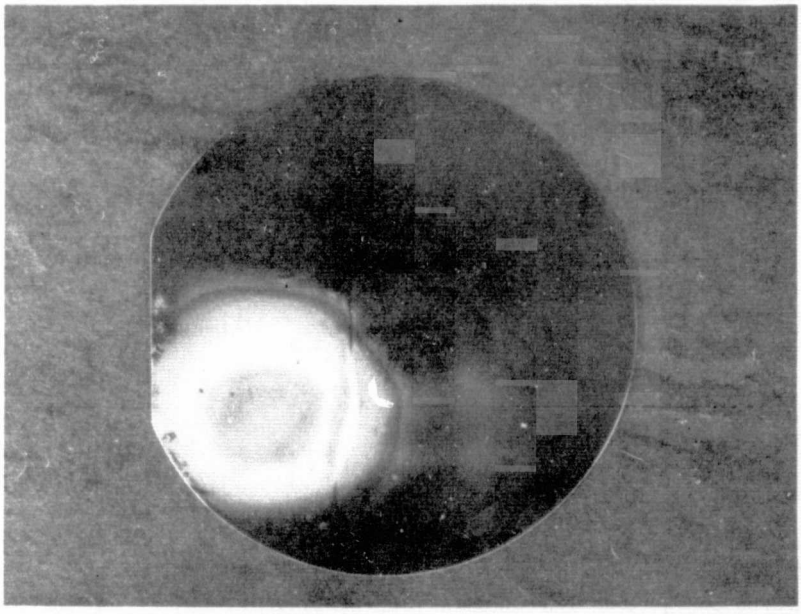

Figure 21. Overall view of sample G16 which was heated in a hydrogen atmosphere. The bright area is heavily etched thermally and is centered at the location where the hydrogen jet impinged upon the wafer.

The results for G17 and G18, run with 100% and 50% nitrogen, respectively, are quite similar. The surfaces are very smooth. The "bulls-eye" film pattern seen earlier for cases mixed hydrogen-nitrogen jet flows is absent. Film thicknesses ranging from 30Å to approximately 150Å are seen, with the thicker films developing near the jet flow.

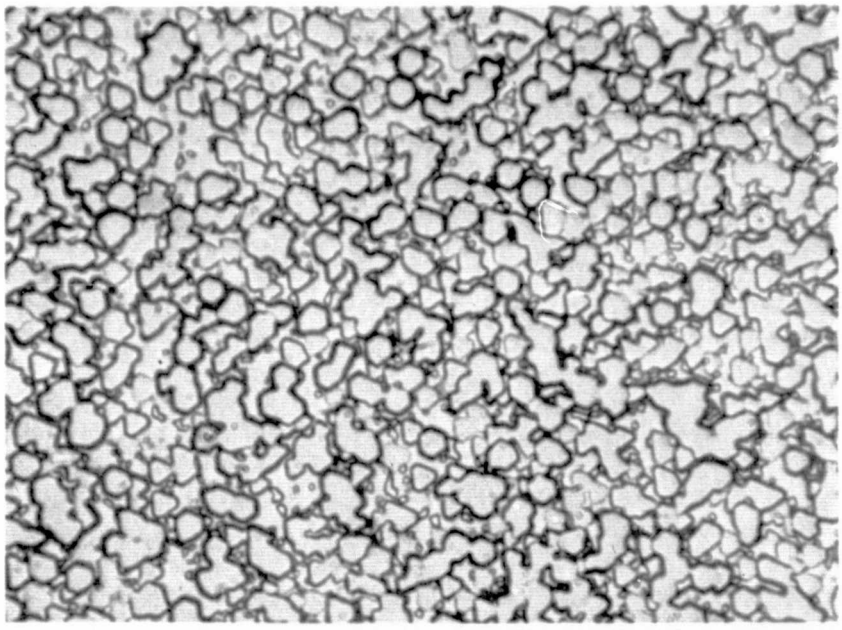

Figure 22. A highly magnified view of the thermally etched region of G16.

Several additional experiments were carried out in a vertical epitaxial reactor (AMT model #800). This experimentation was done to determine whether the results of the gas studies were peculiar to our horizontal reactor or were more general in nature. These are included in Table VIII and are indicated as Runs V2-1 through V2-4. The results for this were gratifyingly similar to those obtained in the horizontal reactor. Sample V2-1, run in hydrogen exhibited severe thermal etching resulting from the high gas flow across the wafer in this reactor. While this result made it impossible to measure film thickness, it is a reasonable conclusion that the rate of any film formation is well below that of silicon surface evaporation, which is quite low at 1080 °C (the equilibrium vapor pressure is 2×10^{-7} Torr.). Runs V2-3 through V2-4, which were run in nitrogen, developed smooth films 30Å-50Å thick. Film thickness increased with both time and temperature, as is shown in Table VIII.

These experiments lead to the conclusion that some surface film forms upon the surface of silicon wafers and thus presumably upon any silicon seed which is heated in the presence of nitrogen. We also identified quartz paper as a serious source of contamination. These experiments have also shown that it is possible to maintain silicon surfaces in a very clean state in pure hydrogen.

4. SESSILE DROP EXPERIMENTS

a. SURFACE FILMS

Sessile drop experiments, designed to determine the compatibility of various tray materials with tin-silicon alloy melts, were undertaken. These experiments consist of melting a drop of tin or tin-silicon alloy upon a substrate of the material in question and the careful observation of the surface of the molten drop. Any scum or film which forms through interaction of the liquid metal with the substrate (because of impurities in the starting tin or for any other reason) will float to the surface of the drop, where, because the specular nature of the liquid surface, it is highly visible. The ability of any proposed tray material to maintain a clean melt surface was quickly and conveniently checked in this manner.

These experiments were performed in hydrogen in the horizontal furnace. We attempted to maintain as clean and controlled an environment as possible. To this end, in the initial experiments, a heavily doped (0.01 Ωcm) silicon slab was used as the susceptor, to avoid any possible evolution of gases from graphite, either by desorption or by reaction with hydrogen to form methane. The susceptor was supported at only three points by its clear, fused-quartz carrier to minimize the production of volatile silicon oxide through the silicon reduction of quartz.

The first substrate was a 1.5 mm thick CZ silicon slice. It was etched heavily in 3:1 HNO_3:HF and dipped in HF just prior to being loaded into the reactor. Any residual oxide on the silicon was removed by a 5 min, 1100 °C firing in hydrogen in situ. The tin piece which had been kept in a cool section of the reactor during this substrate cleaning was loaded onto the substrate after it had cooled to room temperature without any exposure of the substrate to air.

The temperature was then slowly increased. Shortly after the tin melted to form a ball approximately 8 mm in diameter, particles of some foreign material were observed at the surface. These particles were not collected in a single patch but were, instead, distributed over the surface of the ball. They maintained a fixed spatial relationship with each other in spite of vibrations of the tin ball, until the temperature exceeded 900 °C. At 900 °C the particles coalesced into several small scum patches, which circulated rapidly along the tin surface.

The molten drop itself exhibited a singularity in its behavior at approximately 900 °C. The liquid tin maintained a large contact angle with the substrate (did not wet the silicon) for temperatures below 800 °C. But at approximately 900 °C the tin drop wet the silicon and flowed out along the surface, making a contact angle substantially less than 90 degrees.

Both of these observations indicated the presence of a thin, transparent film covering the surface of the molten drop at low temperatures. This film acts to anchor the relatively large visible particles and to prevent direct contact between the liquid tin and the silicon surface. The film seemed to decompose or break up at approximately 900 °C, after which the particles were free to collect in patches and the clean liquid surface can wet the silicon substrate.

We were thus able to detect the presence of a surface film by means of the rather simple sessile drop experiment. The existence of this film under the clean conditions described above indicate the presence of some impurity.

Sessile drop experiments were extended to cover a wide variety of experimental conditions including the following: graphite susceptors; chem-mechanically polished Czochralski-grown (oxygen doped) silicon substrates; sapphire and spinel substrates; acid etching of the tin; and vacuum melting. The tin used was cast in the form of small drops with the improved casting apparatus described earlier. The experimental conditions are outlined in Table IX.

Runs D7 and D8 were performed in hydrogen in the horizontal reactor following the procedures described earlier except that the susceptors used were made of graphite and of silicon-coated graphite, respectively. They were machined from POCO high-density graphite and were cleaned after machining by being fired in vacuum for several hours at 1750 °C. The silicon-sealed susceptor was coated by the decomposition of silane at 1040 °C in a hydrogen ambient. These susceptors went through a standard firing procedure prior to each run to minimize contamination of the tin by desorbed gases. They were heated to 1100 °C in hydrogen and allowed to cool to room temperature, also in hydrogen, thereby baking out adsorbed water vapor and/or oxygen and replacing them with hydrogen.

The results of Run D7 were substantially the same as those observed earlier. Immediately upon melting, the tin surface was covered by a thin film, whose presence was made evident by the fact that the residual small particles on the surface of the tin drop were being maintained in positions that were fixed relative to each other. The film began to break up at 840 °C. The particles showed some small relative motion at 840 °C, indicating that the film was beginning to break up. It was completely gone at 900 °C. As before, the tin drop did not wet the silicon substrate until after the film had broken up. The temperature had to be raised to 1050 °C before the tin flowed out along the silicon surface.

This film interferes with the wetting of clean silicon by tin. While we occassionally observed local, spotty wetting of silicon substrates by the sessile drop at temperatures as low as 500 °C, consistently low contact angles could not be obtained

Table IX

Sessile Drop Experiments

RUN #	SUBSTRATE	SUSCEPTOR	T_{max}	COMMENTS
		A. Hydrogen Series		
D7	Etch-polished FZ silicon	Graphite	1060	Film breakup begins at 840 °C- Film gone at 900 °C - Si substrate wet after film disappears
D8	" " "	Silicon-coated graphite	890	Tilted substrate - Wetting due to motion
D9	Polished Si wafer	" " "	950	Wetting at 725 °C - Film present till 900 °C - 8 Å
D10	" " "	Graphite	950	Some wetting at 500 °C - No wetting in initial contact- Film present till 900 °C - 6 Å
D11	" " "	Graphite	900	Some film breakup and silicon wetting at 750 °C - Film gone at 900 °C - 4 Å
D12	Sapphire	Graphite	900	Breakup begins at 780 °C - Film gone at 840 °C
D13	Spinel	Graphite	970	Tin etched in HCl - Film persists through 970 °C
D14	Sapphire	Graphite	800	Film persists to 800 °C
D14a	Sapphire	Graphite	800	Sample etched in dilute HF - Film persists to 800 °C
D14b	Sapphire	Graphite	970	Re-etch 14a in dil HF - Film persists to 970 °C
D15	Spinel	Graphite	1000	Same sample as D13 - Etched in 50% HNO_3 - Thick crust which disappears at 800 °C - Film persists to 1000 °C
D15a	Spinel	Graphite	1050	Re-etch D15 in 3% HF - Film still present at 1050 °C
		B. Vacuum Series		
V1	Sapphire	Mo	950	Wispy film circulating on drop surface
V2	Sapphire	Mo	1025	Film visible upon wetting - Film breaks up at 1025 °C
V3	Etch-polished FZ silicon	Mo	820	Film visible upon melting - Film coalesces into a single patch at 820 - Wetting at 820 °C

until the tin had been heated to 900 °C to remove the film. Figure 23 is a SEM view of a 2 mm tin drop that was melted upon a float-zone silicon substrate and heated to 600 °C. An especially thick portion of the film is evident at the center and across the left side of the drop. The poor wetting is shown clearly by the contact angle, which is greater than 90°.

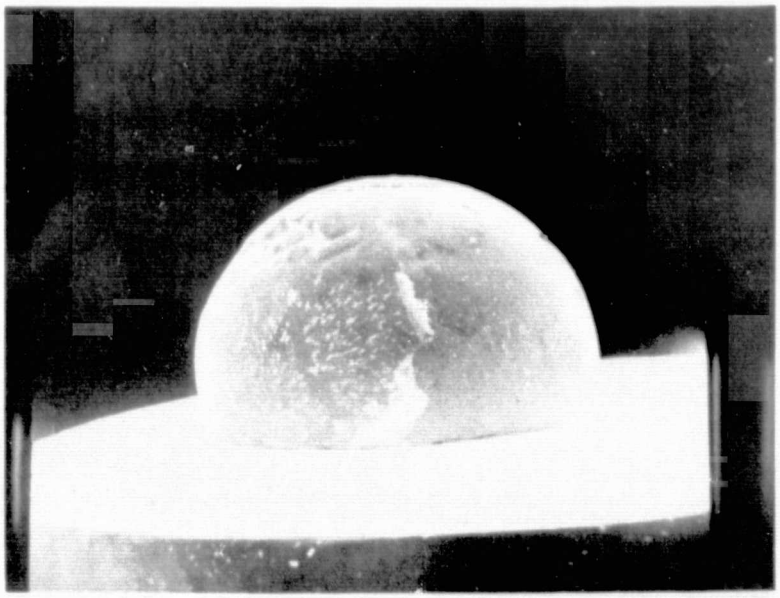

Figure 23. Profile view of a 2 mm tin drop

Run D8 provided clear evidence that it is more difficult for the tin drop to wet the silicon over the area of initial contact than on the area of later contact. The substrate in this case was tipped slightly. At 900 °C the tin drop rolled from its initial location, where the wetting was limited to occasional spots along the dot periphery, to a new position, where it flowed out across the surface. This may be seen in Figure 24. The circular area of unwet silicon, where the tin drop first sat upon the wafer, is clearly outlined by the small tin dots left behind by the rolling drop. The surface film which covers the top surface of the drop must also be present at the tin-silicon interface at the bottom, thereby preventing the direct tin-silicon contact required for wetting.

The similarity of the results obtained with the graphite susceptor to those obtained with the silicon susceptor indicates that the graphite introduces no additional contamination. All subsequent sessile drop experiments performed in hydrogen, therefore, used the graphite susceptor.

Czcochralski-grown, chem-mechanically polished wafers were used in Runs D9 through D11. Ellipsometer measurements made upon the portion of the substrate not covered by the sessile drop itself indicated 4 Å to 8 Å film on the silicon - the thicker number being obtained after the sample was exposed to air for two hours and the 4 Å result within ten minutes of the silicon being removed from hydrogen. These clean surfaces serve as confirmation that incoming gas supply is not contaminating the tin drop.

Figure 24. Photograph of Run D8. The small, circular area of initial contact is clearly visible.

The behavior of the tin drop was quite similar to the earlier results. The tin surface film was always seen upon the tin's melting. It persisted up to 900 °C, after which it seemed to disappear. The film always began to break up below 900 °C (in the case of D11 it began to break up as low as 750 °C). These polished wafers were wetted by the tin drop at consistently lower temperatures than were the etch polished wafers (in one case [D10] the wafer was wetted at as low as 500 °C). It is not clear whether this is caused by the difference in surface configuration or in some way by the bulk oxygen doping.

A series of Runs (D12 - D15) was made using single-crystal sapphire and spinel as substrate materials. These substrates were heated in hydrogen at 1100 °C for ten minutes prior to being loaded with the tin charge, exactly as were the silicon substrates. Runs D12 and D14 used tin directly as cast, and a variety of acid etches were used in attempts to clean the tin surface for the others. The details are given in Table IX.

The results obtained in D12 with unetched tin are similar to those with silicon substrates. A film forms at low temperature, begins to break up at an intermediate temperature, and disappears at some final, higher temperature. In this case, the breakup and disappearance were observed at 780 °C and 840 °C, as measured with the optical pyrometer. The differences between these temperatures and the values seen with silicon are, more than likely, results of the emissivity difference between the flat silicon substrate and the rounded tin drop.

All attempts to remove the surface film by acid etching, either before or after heating of the tin, were unsuccessful. The acids tried were HCl, HF, and HNO_3. In all cases where the tin was exposed to an etch, the film persisted well beyond 900 °C. Thus, etching did not appear to be a useful procedure for cleaning tin and was not used further.

Several experiments were performed in vacuum to determine whether the ambient has any substantial effect upon the behavior of the tin drop. The vacuum system was pumped by a well-trapped mercury diffusion pump. The background pressure during these experiments was in the range 2×10^6 to 5×10^6 torr. A molybdenum slug, which had previously been fired at 1750 °C in vacuum, was used as the susceptor. (These experiments are summarized in Table IX under the subheading "Vacuum Series.")

Coherent films were seen on the surfaces of the tin drops after melting, a phenomenon exactly like that observed for heating in hydrogen. At higher temperature the drop surface cleaned up, again, a phenomenon like that seen in hydrogen. The details of the cleanup were, however, different for vacuum heating. In this case the behavior was more varied. The film of Run V2, where the substrate was sapphire, seemed to break up and disappear at 1025 °C. With silicon as the substrate, the film which had initially covered the entire surface of the drop coalesced into a single patch at 820 °C, leaving the rest of the surface bright and clean.

Figure 25 is a SEM photograph of the surface of a tin drop that was supported by a float-zone silicon substrate and heated in hydrogen to 500 °C. The film is clearly shown by the speckled appearance of the surface. The cracks in the film (the clear dark areas) are probably the result of differential thermal contraction of the film and the tin drop.

Figure 26 is another SEM photograph of the surface of a tin drop heated to 800 °C on silicon. The film in this case is at the stage where it is partially broken up. The surface film, which initially completely covered the tin surface, as in Figure 25, has changed to an open, lacy structure, and large, open patches of clean tin are clearly visible. The dark triangular or hexagonal areas are silicon platelets that regrew upon the drop surface.

Attempts were made to analyze the film by means of electron beam excited X-Ray fluorescence and Auger spectroscopy. The X-Ray fluorescence showed only silicon and tin and was thus rather inconclusive.

Auger examination of a film-covered region of a drop surface showed the presence of large amounts of oxygen, carbon, and a small amount of silicon in addition to tin. The same measurements at a clean portion of the drop yielded much smaller oxygen and carbon signals. Silicon was completely absent. The film-covered

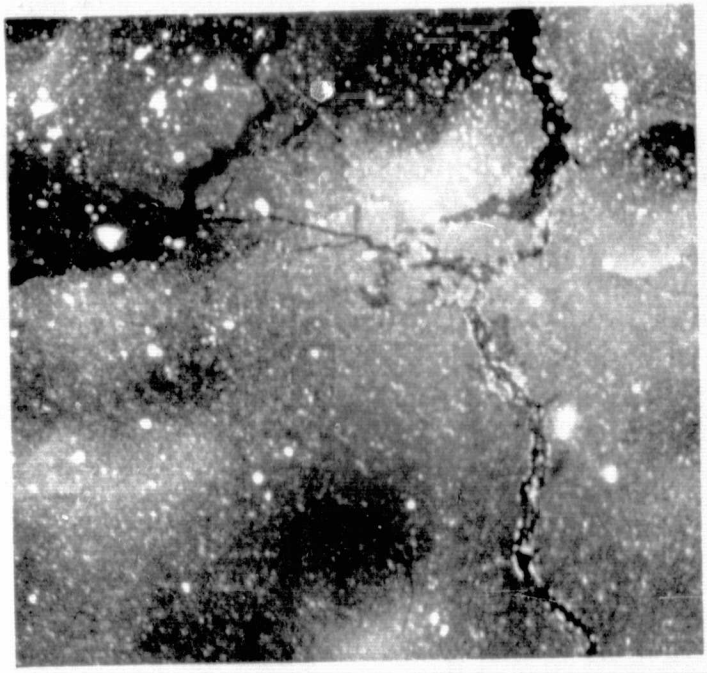

Figure 25. SEM photograph of surface film on a tin drop heated to 500 °C.

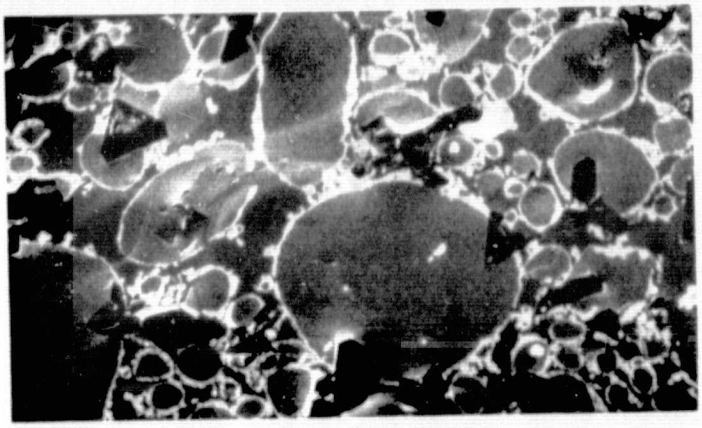

Figure 26. SEM photograph of the surface of a tin drop heated to 800 °C

region was sputter-etched to a depth of less 200 Å. Following this, silicon and carbon were completely absent, and the oxygen level was reduced by a factor of 10.

The appearance of a film on the surface of tin drops independent of substrate and of ambient suggests that the impurity causing the film is present as a contaminant in the tin itself. The Auger experiments indicate that the film is less than 200 Å thick and that it consists of a mixed oxide of silicon and tin.

b. SURFACE DENDRITIC GROWTH*

The tin drop of Run D10 was examined carefully to study the nucleation and growth of silicon crystals out of solution at the liquid surface. The tin drop, supported by a silicon wafer, had been heated to 950 °C, held at temperature long enough to have become saturated with silicon, and then quenched by dropping the RF heating power to zero. Most of the observations were made with the scanning electron microscope, although the optical microscope was used occasionally to determine the flatness of a particular crystal.

A high density of surface crystals - presumably nucleated by foreign particles - was observed. Two views of portions of the droplet surface are given in Figures 27 and 28. The surface density of nuclei is approximately 3×10^4 cm^{-2}. A wide variety of crystalline shapes is especially evident in Figure 28. A detailed analysis of these structures suggests that the initial seed has the form of a twinned triangular nucleus. The twin plane is (111), and the vertex angles of the triangle are in the $[\bar{1}12]$, $[2\bar{1}1]$, and the $[1\bar{2}\bar{1}]$ directions. The crystals have only one twin plane and, after the completion of the triangular form, have a ridge extending completely around the median plane. These triangles grow very slowly thereafter, since there is no outward-facing reentrant edge to act as a good nucleation site. Many of these forms are seen in Figures 27 and 28.

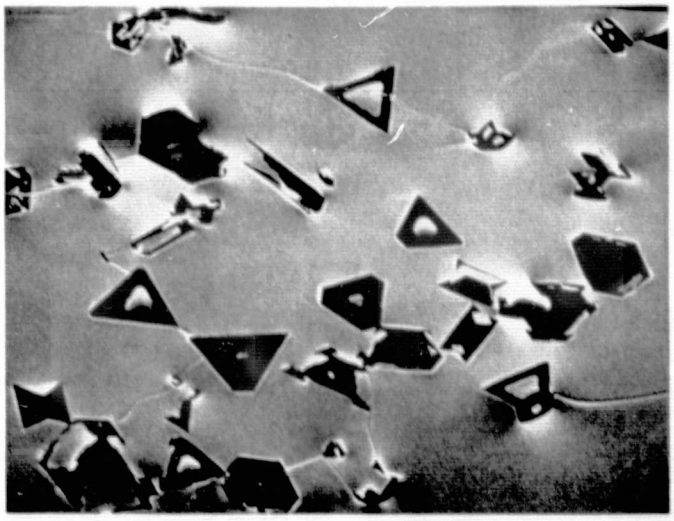

Figure 27. Surface View of Silicon Crystals Nucleated and Grown by Rapid Cooling of a Saturated Alloy Droplet, 400X Magnification

*The crystallographic analysis was performed by Professor J.W. Mitchell.

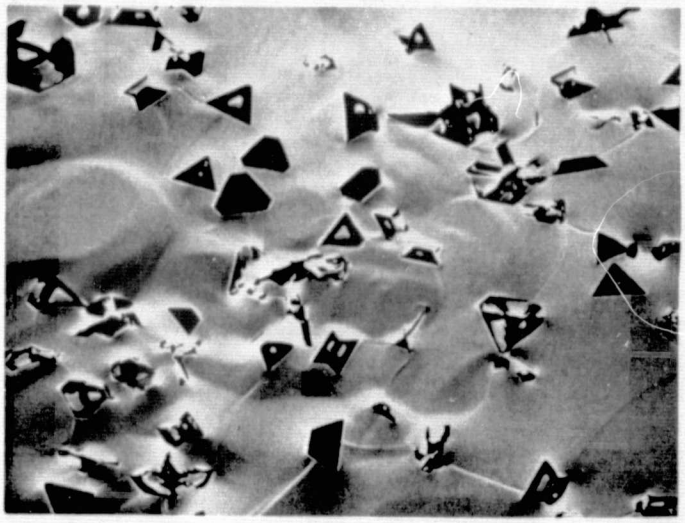

Figure 28. Silicon Crystals Grown at the Surface of a Rapidly Cooled, Saturated Alloy Droplet, 270X Magnification

In most cases, continued growth of these surface crystals, after the completion of the triangle, proceeds by linear growth of dendritic leaders out from the vertices of the triangle along the coplanar system of <110> directions. This process is shown schematically in Figure 29. Photomicrographs of crystals showing this development, as well as further stages of growth, are presented in Figures 30, 31, and 32.

In Figure 29, ABC is the crystal at the completion of the triangular growth stage. The edges AB, BC, and CA lie along the $[\bar{1}01]$, $[0\bar{1}1]$, and $[10\bar{1}]$ directions and have outwardly projecting ridges defined by the intersections of the $(11\bar{1})$, $(\bar{1}11)$, and $(1\bar{1}1)$ planes with their mirror images in the (111) twinning plane. The external angle between the planes bounding the ridge is 219°.

The completion of the development of the triangular nuclei is characterized by the formation of sharp corners at the vertices of the triangle. It is also accompanied by an increase in the local supersaturation, which, when large enough, causes the outward growth of two dendritic arms along the $<1\bar{1}0>$ directions radiating from these corners. For the singly-twinned crystal, one side of these arms is sharply defined by the line of intersection of two $<1\bar{1}1>$ planes. For example, the dendrite along AD has a straight edge within the acute angle DAJ defined by the intersection of the $<1\bar{1}1>$ plane with its mirror image in the twin plane. This pair of planes forms a ridge. Rapid growth along the $<1\bar{1}0>$ directions is driven by the reentrant which has the largest projection along the corresponding $<1\bar{1}0>$ axis. For

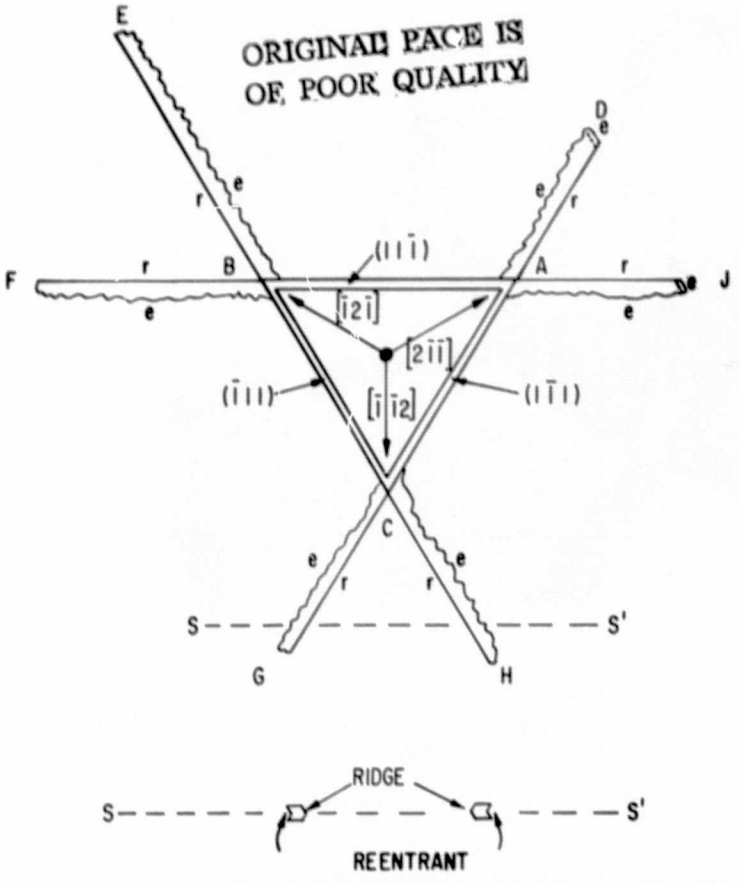

Figure 29.

Schematic Representation of Twinned Linear Dendritic Growth Occurring at the Corners of a Twinned (111) Twinned Nucleus. The surfaces that are ridges and reentrants are indicated by "r" and "e", respectively. A cross section through a pair of dendrite arms shows the ridged and reentrant pairs of planes.

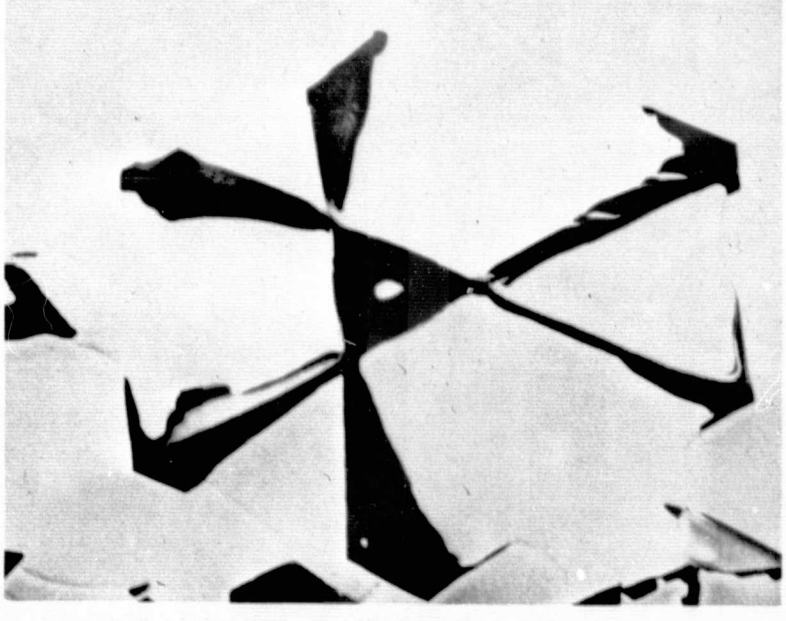

Figure 30. An Example of Linear Dendritic Growth Proceeding from the Corners of the Triangular Twinned Crystal

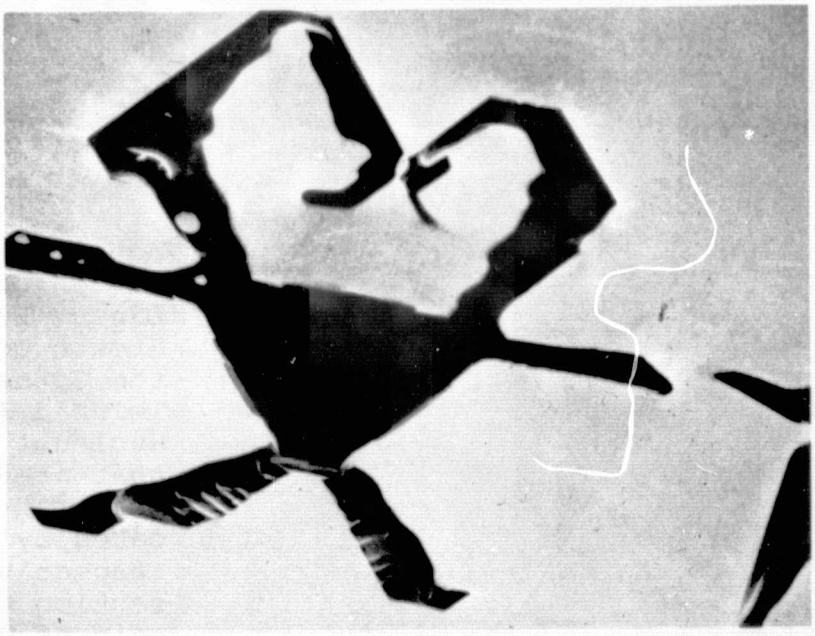

Figure 31. Silicon Crystal Development from the Triangular Nucleus, Including a Dendrite Direction Change of 60°

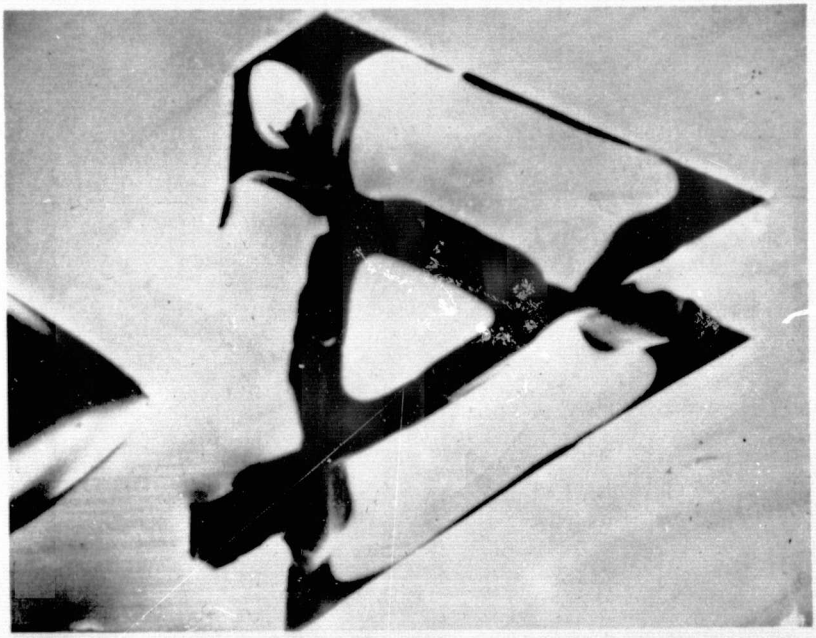

Figure 32. Silicon Crystal Development Showing 120° Changes in the Direction of Dendrite Growth.

example, the linear growth along AD is driven by the reentrant formed by the intersection of the $(1\bar{1}\bar{1})$ plane with its mirror image in the twin plane. This process is shown schematically by the sharp angles terminating the growth at D and J and by the dotted lines, which indicate the intersections of the $(\bar{1}\bar{1}\bar{1})$ plane with its twin plane at D and J. Crystal formation resulting from this reentrant set has a component directed toward the $(\bar{1}11)$ ridge and will, therefore, result in long, thin, straight-line dendritic growth.

There are two ways in which the rapid outward growth of the dendritic leaders can be terminated: (1) by extension of the length of the reentrant at D in a direction parallel to CB and (2) by the growth of a ridge parallel to BA and the elimination of the reentrant. These are shown in Figures 33(a) and 33(b). The first of these processes may be repeated as shown in Figure 31.

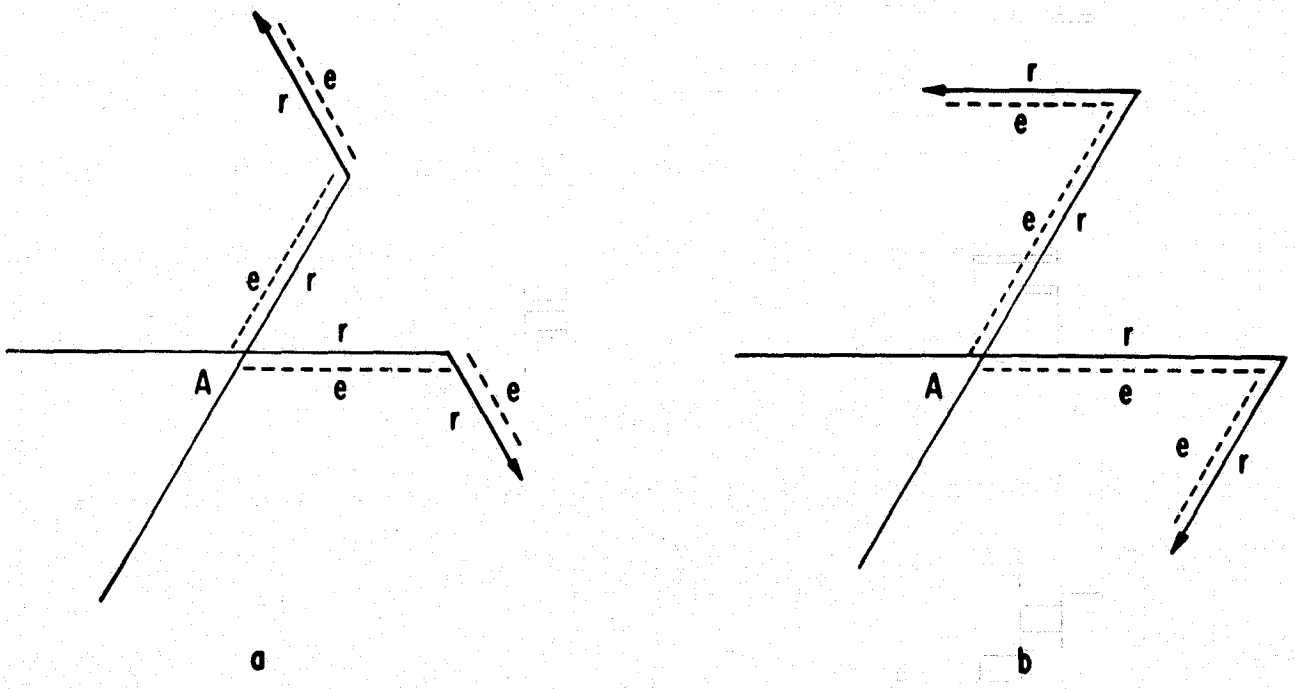

Figure 33. (a) Schematic Representation of Dendrite Development Following a 60° Change in Direction; (b) Schematic Representation of Dendrite Development Following a 120° Change in Direction

In the first process, the growth direction of the dendrite changes successively through an angle of 60°, and with each rotation an outward-facing ridge changes into a reentrant and vice versa. In the second case, the growth direction changes through 120° with the outer edge a continuous ridge, and the process develops an internal 60° angle, as shown in Figure 32. When this occurs, there is a strong tendency for a thin dendrite to be developed colinear with the ridge, which propagates until this dendrite intersects the $\langle 1\bar{1}0 \rangle$ dendrite growing from the opposing vertex of the initial triangle. At this point, both

dendrites cease growing, being terminated by outward-facing ridges. There is some indication in Figure 32 of thin web growth which is filling in the acute 60° included angles defined by the change in dendrite growth direction. This is to be expected, since the interiors of both of these dendrites are reentrants.

An especially well-developed case of planar growth from the reentrant side of one of these linear dendrites is shown in Figure 34. The internal angle on the left side of the crystal, which has inward-facing reentrants, has partially filled up with a thin web of silicon. Presumably, the other areas bounded by the dendritic web would have done the same had there been enough silicon and had the reentrant growth surfaces been clean enough. This crystal gives clear evidence that dendritic growth and web development is possible on the surface of a supersaturated solution of silicon in tin.

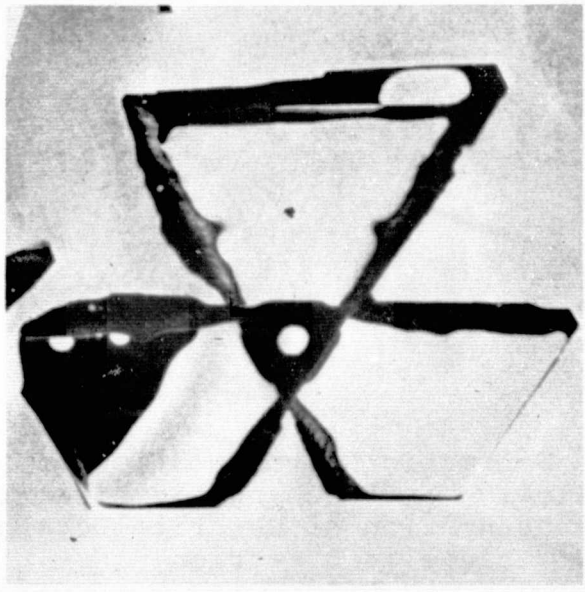

Figure 34. An Example of Surface Growth. A thin web grew along the surface of the melt from the reentrant sides of the linear dendrites.

The crystal shown in the optical photograph of Figure 35 provides another example of this development. The crystal ACHQRJ has developed between the two dendritic directions AJ and CH by a process in which the ridge QR has grown farthest from the nucleus.

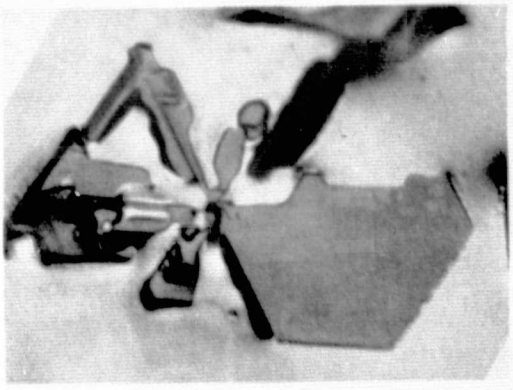

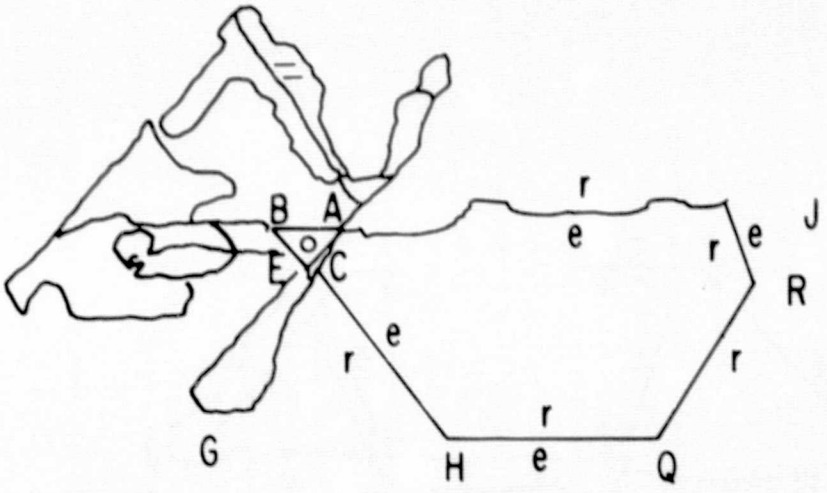

Figure 35. An Example of Planar Growth

This development seems to imply that the inner surfaces of the dendrites AJ and CH, which have reentrant character, were involved in the nucleation and growth process which propagated a thin silicon crystal along the ridge (parallel to AC) from the intersection with the reentrants.

Crystal ACHQRJ, a particularly perfect crystal, appears to have developed by stable, steady state growth from the original dendritic nucleus. The crystal was pale orange-yellow after the double transmission of the beam through it. Examination of this crystal with intense dark field illumination showed a uniform plane, parallel plate which, apart from an area along AJ, had no surface or internal terraces, holes, or other imperfections. This finding was confirmed by the absence of interference contrast.

In most cases continued crystal growth proceeded by the growth of linear dendritic leaders out from the vertices of the completed triangle, along the coplanar system of <110> directions, and by the subsequent growth of planar web from the reentrant sides of these dendritic leaders. However, another type of crystal growth was observed to take place. This is the

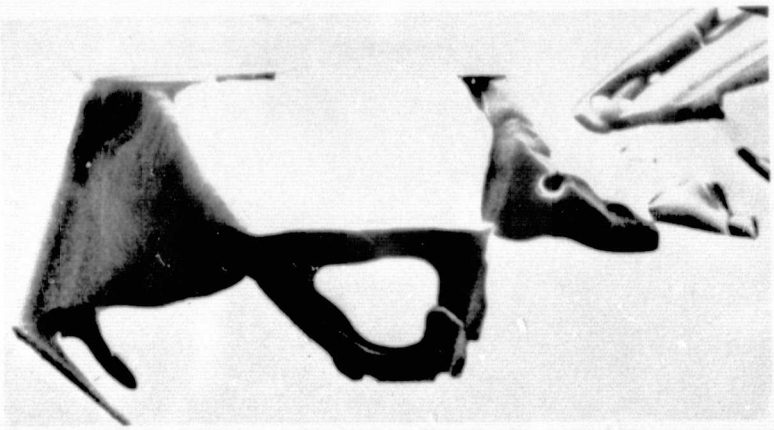

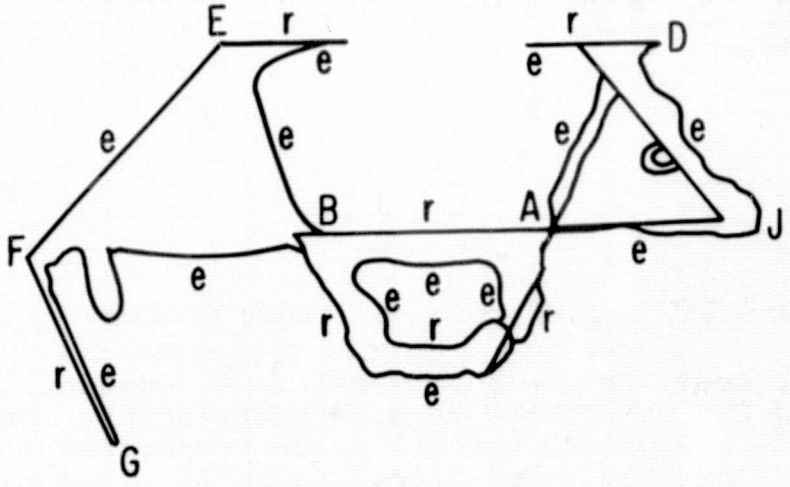

Figure 36. Crystal Exhibiting Planar Growth in a <$\bar{1}\bar{1}2$> Direction, Nucleated by a Re-entrant Twin Pair

filling in of the acute angle between the dendrite arms extending from the completed vertices of the triangular nuclei. Crystals in which this type of growth has occurred are shown in Figures 36 and 37.

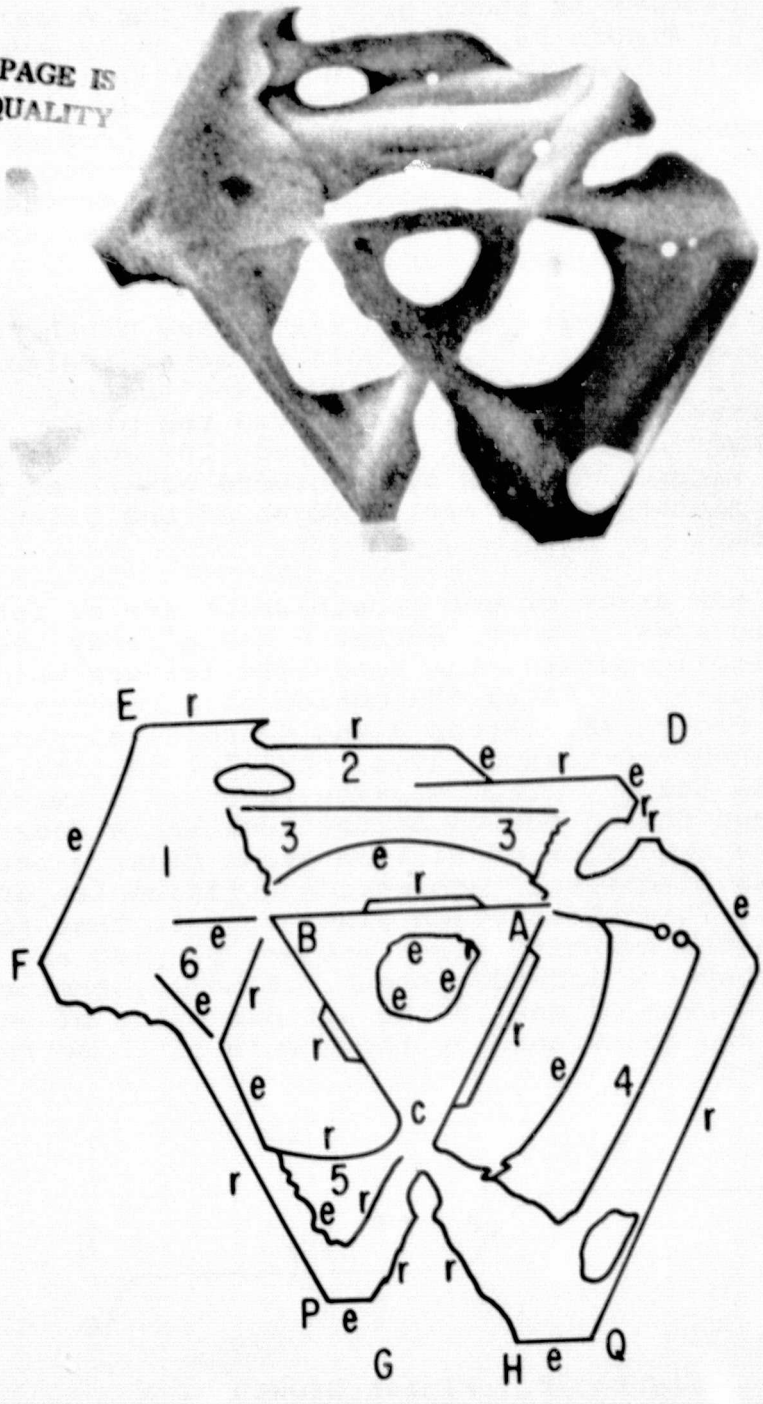

Figure 37. Crystal Showing Many Aspects of Surface Growth

The basic process is shown occurring at the A and B corners of the nucleus in Figure 36. The triangular units AJD and BEF have outward facing reentrants, which will facilitate two-dimensional growth in the absence of adsorbed contamination. A slowing down of outward growth, possibly resulting from an exhaustion of the supply of silicon atoms and associated development of contamination, is followed by an increase in supersaturation at E and F and the development of the dendritic leaders with outward facing ridges along ED and FG.

The crystal of Figure 37 illustrates many of the growth features previously described, as well as several significant new features. It thus provides a convenient summary. The acute angle at the vertex at B has filled in via the planar growth process just described. It has developed 120° angles at E and F, as shown in Figure 36. The slow outward growth at the centers of the ridges defining the exterior edges of the triangular nucleus is quite evident.

There are six areas of web growth which are of interest. The planar growth in area 1 at the corner B has already been discussed. Area 2 is developing outside the dendritic leaders which defined the ED edge parallel to BA by the motion of a reentrant edge toward D, as shown in Figure 38. Areas 3 and 4 are developing by the motion of the inner reentrant edges, parallel initially to BA and AC toward BA and AC. The relative rates of outward motion of the ridges and inward motion of the reentrants under the influence of the same flux of silicon atoms clearly establish the relative two-dimensional nucleation efficiencies of ridges and reentrants. This observation also suggests that screw dislocations in the twinning plane are not playing any significant role, if they are indeed present. Finally, the areas at 5 and 6 show the growth of web in the net direction of an outward ridge bridging two reentrants by the growth of those reentrants toward each other.

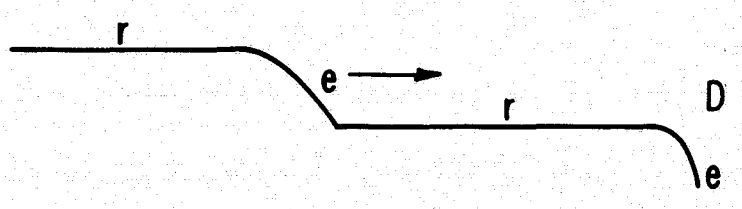

Figure 38. Planar Growth of a Reentrant Edge

While the planar crystal growth just discussed has been quite small (less than 0.1 mm in extent), it establishes the essential feasibility of the process from a fundamental physical viewpoint, for it shows that thin planar crystals can be grown from a solution of silicon in tin by surface nucleation and growth processes.

5. SURFACE GROWTH

a. MODEL-I

The Floating Substrate Process involves the deposition of silicon from the vapor phase upon a layer of silicon which floats on an underlying tin-silicon melt. Growth is initiated from the edge of a seed crystal and is induced to propagate over the surface of the melt by the application of thermal gradients and silicon deposition rates which produce the required degree of supersaturation. The crystal is withdrawn at a rate equal to the growth velocity to maintain the growth edge at a fixed position in the furnace. An essential feature of this process is growth over the surface of the tin-silicon melt of a thin single-crystal sheet, nucleated from the edge of the seed crystal. A surface growth apparatus was constructed and operated to investigate the problems associated with this aspect of the Floating Substrate Process.

Figure 39 shows the initial version of the apparatus used to study surface growth. Its design features included provision for electromagnetic pumping of the liquid metal and thermal gradients which inhibit crystal growth upon the crucible walls.

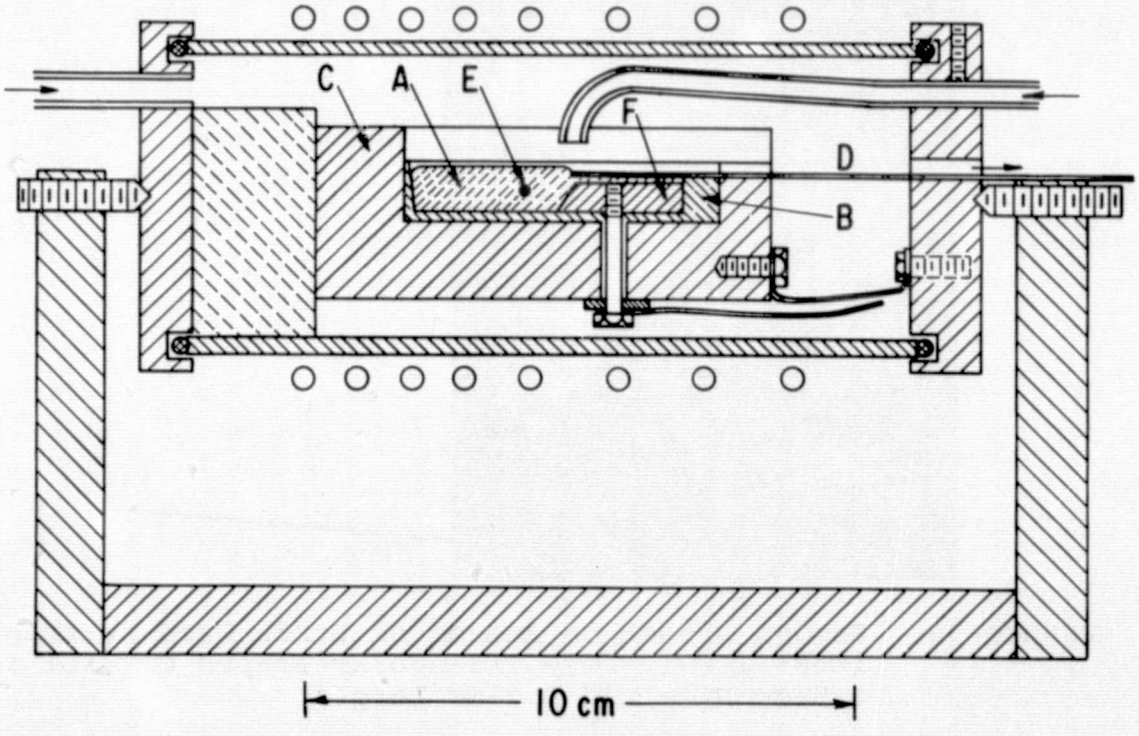

Figure 39. Side View of the Surface Growth Apparatus

Referring to this diagram, melt A is contained in a tray B made of boron nitride. It is heated by a graphite susceptor C, which is designed so that the left end of the tray (as well as its side edges and bottom) will be held at a higher temperature than the end where seeded growth takes place. This temperature distribution is aided by graphite side rails, which form a part of the susceptor and overhang the edges of the tray to help maintain a high temperature along the edges. The growth region is cooled by radiation and by a gas jet which can be directed against the melt surface near the end of the seed crystal. The seed D is introduced through an opening in the right end of the furnace and floats on the surface of the melt. Forced circulation in the melt can be produced by passing a current between a tungsten wire, E, and an electrode, F, which is positioned at the right end of the tray in the presence of a transverse magnetic field. This electrode, made of graphite or tungsten, is wetted by the alloy so that a thin layer of liquid is drawn into the thin space between D and F. This layer is made thin so that excess Si in the alloy will be able to diffuse to the overlying seed, rather than form a deposit on the electrode.

The results obtained in some of the early experiments conducted with this furnace are shown in Figures 40 and 41.

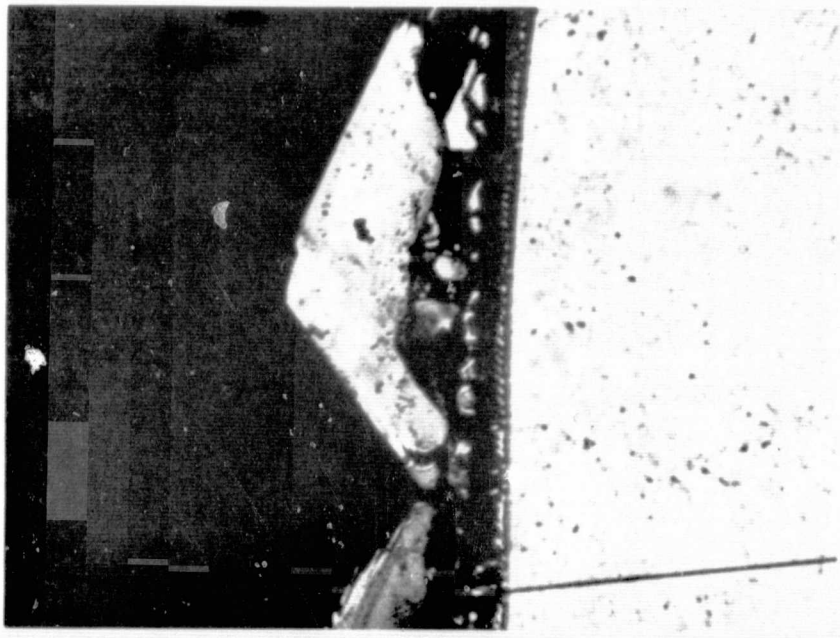

Figure 40. Seeded Growth on End of Si Strip Used in Experiment SGF-1. The Triangular-shaped Crystal is 0.5-mm Wide and 0.2-mm Long.

For Experiment SGF-1 the furnace was loaded with 40.1 g of Sn and raised to 920 °C. A strip of Si 13 mm wide and 0.4 mm thick, and having its long axis in the <110> direction, was fed in through the slot in the end plate to bring the melt to

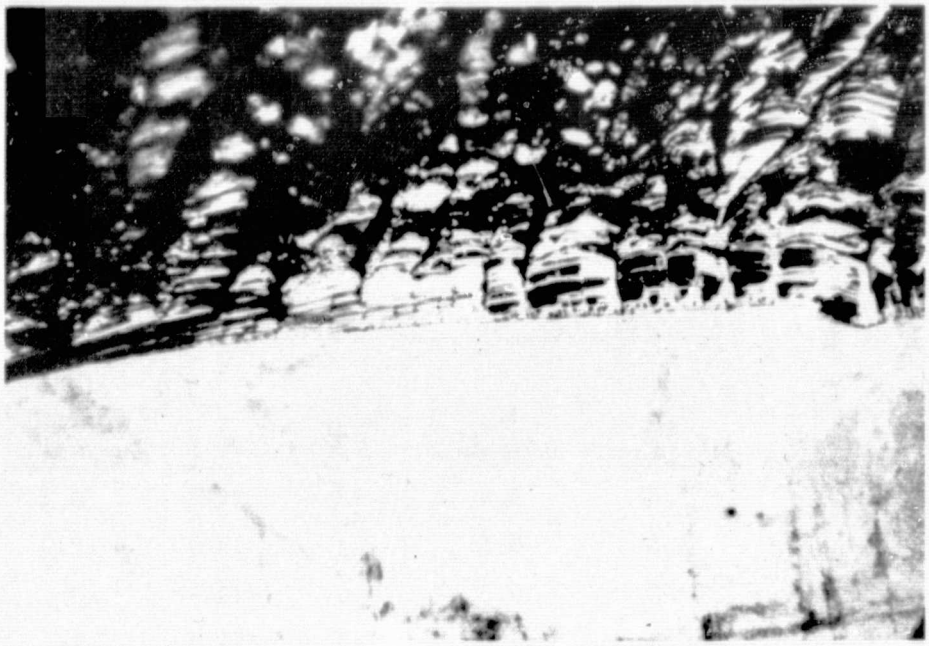

Figure 41. Region of Single Crystal Growth Formed on the Strip of Si Used in Experiment SGF-2. This Region Is Approximately 2-mm Wide and 0.5-mm Long

saturation; the furnace controls were adjusted in an attempt to cause some Si to regrow on the end of the strip. When the experiment was completed, the excess Sn was removed from the strip, and it was found that only a slight amount of growth had taken place, as shown in Figure 40. This growth took the form of a number of tooth-like extensions of the strip, each about 0.5 mm wide and 0.2 mm long. The upper faces were (111) planes approximately tangent to the upper side of the strip. The lower side which faced down toward the melt was terraced by a series of faceted steps.

In Experiment SGF-2, a crystal was grown using the same charge with more Si added by dissolution from the strip. This experiment resulted in the growth shown in Figure 41. Most of the growth was polycrystalline, but an area of single-crystal growth 1.5 mm wide and 0.5 mm long was produced at the end of the strip, with a flat (111) upper surface almost coplanar with the upper surface of the strip. The columnar appearance of this region suggests that growth was initiated at a multiplicity of points along the edge of the strip, so that each growth area started with its upper (111) surface at a slightly different elevation. This produced slight growth steps at the boundaries where these crystallites merged together, giving the columnar appearance.

The results of further growth experiments using this furnace arrangement are summarized in Table X. The last two columns indicate the amount of silicon that was grown during each experiment. The first of these gives the total length of the polycrystalline layer that was produced. The other indicates the length of crystal that appeared to have the same orientation as the seed crystal and could be described as "seeded growth." It is evident that very little of the silicon that has been grown was nucleated by the seed crystal.

Table X

Growth Furnace Experiments

Expt. No.	Wt Sn (g)	N_2 (ℓ/min)	H_2 (ℓ/min)	I_{stir} (A)	Seed	Total Growth (mm)	Seeded Growth (mm)
1	40.1	3.3	8.4	+2	(110)	0.2	0.2
2	Reused	2.3	6.5	-4	(110)	12.	0.5
3	Reused	3.3	6.3	-5	$(\bar{1}\bar{1}2$	9.	0
4	Reused	3.8	5.5	+5	$(11\bar{2})$	1.	0.5
5	Reused	3.8	2.4	+4	Web	~ 0.5	0
6	38.6	2.4	0	-1	$(\bar{1}\bar{1}2)$	9.	~0.5
7	10% Pb	3.3	4.6	0	(110)	8.	0.2
8	37.5	3.3	0	-2	$(\bar{1}\bar{1}2)$	10.	~0.1
9A	Reused	1.6	2.4	+1	$(\bar{1}\bar{1}2)$	8.	0
9B	Reused	0.8	4.6	-1	$(11\bar{2})$	32.	0
9C	Reused	1.4	4	-1	(110)	45	0
9D	Reused	1.6	3.5	-1	Web	32	~2.

During these early experiments it was found that rapid growth could be achieved by directing the cooling jet so that it impinged on the melt surface just ahead of the growing edge of the solid silicon, resulting in growth velocities of 5 to 6 mm/min. The surface growth was thin enough that it could easily be seen to bend as the seed crystal was moved during the growing operation, but it was composed of many small crystals which had little relation to the orientation of the seed crystal used to initiate growth.

The operation of the surface growth apparatus is shown in Figure 42. In this experiment, SGF-11D, a layer of silicon 35 mm long was grown, but it separated from the seed as it was being drawn off. The furnace was then shut down so the results could be photographed. In addition to the polycrystalline ribbon of silicon that was being grown on the end of the seed crystal,

there was another "peninsula" of silicon, approximately 6 x 12 mm in size, which could be seen growing out from the corner of the boron nitride tray. Elsewhere over the surface of the tin were small silicon crystals which formed as the system was cooling down.

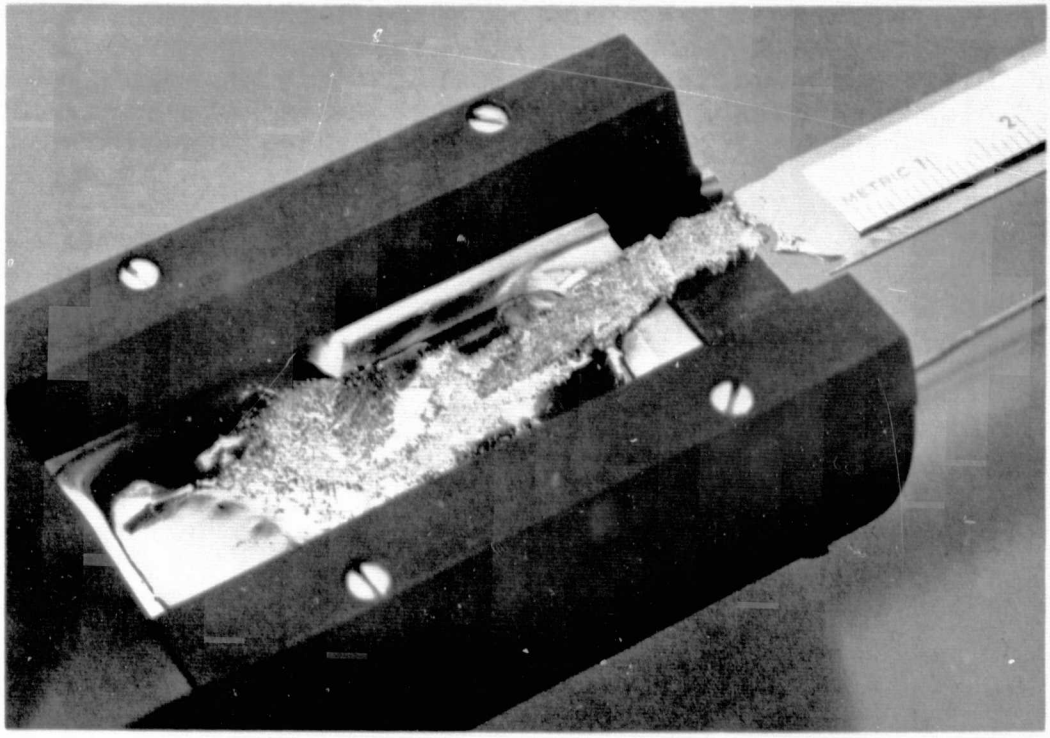

Figure 42. Crystal growth produced during SGF-11D. The furnace was shut down after the growth separated from the seed crystal. An area of unwanted growth extends toward the viewer from the corner of the boron nitride tray.

This furnace had several shortcomings that needed to be corrected. The most serious difficulty was that a layer of foreign material, or scum, always formed on the surface of the Sn-Si alloy and interfered with the growth process. Most of it could be blown aside by the gas jet, but there always appeared to be some attached to the end of the seed crystal. It seemed probable that this scum formation was the principal reason for our failure to achieve single-crystal growth.

The origin of the scum was not clear, but there appear to be several potential sources. The graphite susceptor may absorb oxygen or other gases while the furnace is open, resulting in the evolution of CO during operation and thus leading to the formation of SiC on the melt surface. Also, reaction with the boron nitride tray may produce a film of BN on the melt surface. In addition, there are several places where hot quartz was in

contact with the graphite susceptor. Since these materials have been observed to react with each other, their products might have contributed to the scum.

Another problem was that, while the gas jet provided an effective means for cooling the melt surface, it also caused the surface of the melt to flow in an uncontrolled manner, with the result that it was impossible to isolate the effect of melt circulation on crystal growth. It appeared that a cold finger, placed close to the surface of the melt, would provide a better means for achieving local cooling ahead of the growth edge.

b. MODEL 2 -- MOLYBDENUM SUSCEPTOR

A new susceptor, which was expected to eliminate the stated difficulties, was constructed next. Figure 43 shows a cross-section view of this modification.

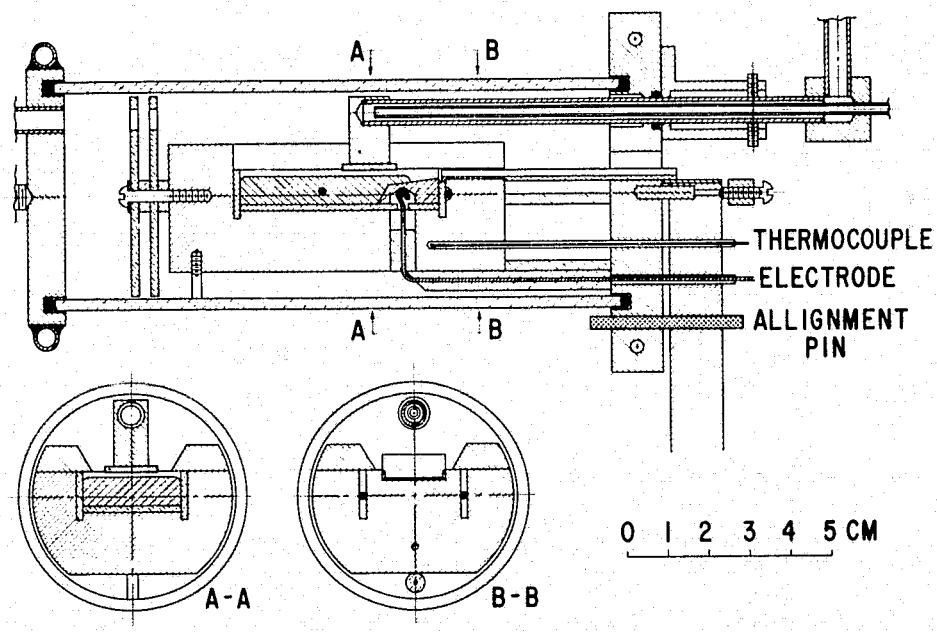

Figure 43. Surface Growth Furnace With Molybdenum Susceptor.

The susceptor consisted of a block of molybdenum, which was slotted so trays of various materials could be evaluated for their suitability for melt containment. The tray was made in the form of a shallow box, with sides fitting together snugly around a bottom plate and held together by the slots of the susceptor. Trays made of quartz, alumina, sapphire, beryllia, or tungsten could be obtained readily in this way. Electrodes for electromagnetic stirring were also provided. Local cooling was produced by a water-cooled copper cold finger having a sapphire plate -- which could be adjusted to be in close proximity to the melt surface -- attached to its lower surface. A boron nitride trough was also provided to facilitate the withdrawal of the silicon through the exit port. A thermocouple and chart recorder were added for more convenient operation and data-taking.

This modification of the surface growth furnace permitted operation in a pure hydrogen atmosphere and eliminated all construction components that were suspected of generating reaction products during operation.

SGF-16 was an initial test run with quartz as the tray material. It was loaded with a 40-gram charge of tin which had been precast under hydrogen in a boron nitride cup. The usual silicon dioxide "fluff" was observed as the tin was heated through the 800 to 1000 °C range. With further heating, the fluff gathered together and was blown out of the field of view. Thereafter, the tin surface appeared bright and clean. Then 1.15 g of silicon were added and brought into solution near 1100 °C, and a seed was introduced in an attempt to induce surface growth. The visibility was poor because the gas conduction cold finger was being used to produce the local cooling. A slight amount of growth was obtained. As the crystal was drawn outward, however, it was seen that liquid was running out of the tray, so the furnace was shut down. Subsequent examination showed that some of the alloy which had been drawn out with the seed had made contact with the susceptor and formed a capillary bridge, which had siphoned much of the alloy out of the tray.

The furnace was cleaned and reassembled with a sapphire tray. The boron nitride exit slide was modified so that it shielded the susceptor from possible contact with the tin alloy, and some metal was cut from the header plate to improve the visibility under the cold finger. The furnace was then heated to 1200 °C in hydrogen to bake out the system and to make sure that the tray would survive the thermal cycle without breakage.

For SGF-17 the furnace was loaded with 41.9 g of tin, heated to 1200 °C, and returned to room temperature twice. This time there was no evidence of fluff formation. The tin surface appeared clean except for a very small patch of scum, which appeared to have been introduced with the tin. It was no larger during the second heating cycle and did not increase with time at the operating temperature. Subsequently, 1.065 g of silicon was added, and the power was varied up and down several times to permit observations of spontaneous growth. During one of these cycles a platelet formed on the melt surface and grew to about 2 mm diameter. It had a specular surface with well-defined hexagonal facets, indicative of improved crystal growth conditions. After the crystallized silicon had been remelted, a seed having a <111> axis and $(11\bar{2})$ principal faces was introduced, spliced to the melt, and growth was initiated. Because of difficulties with the cold finger, only about 8 mm of growth was achieved before it was necessary to halt the experiment. The resulting growth is shown in Figure 44. It contains a region about 3 mm by 5 mm where the growth is substantially single and has the same crystallographic orientation as the seed. This photograph was taken with directional illumination reflected off the areas of oriented growth, causing them to be strongly highlighted. This was the first time that extensive areas of seeded growth were obtained,

and it indicated that the changes associated with the introduction of the molybdenum susceptor and the sapphire tray had greatly improved the growth conditions in the furnace.

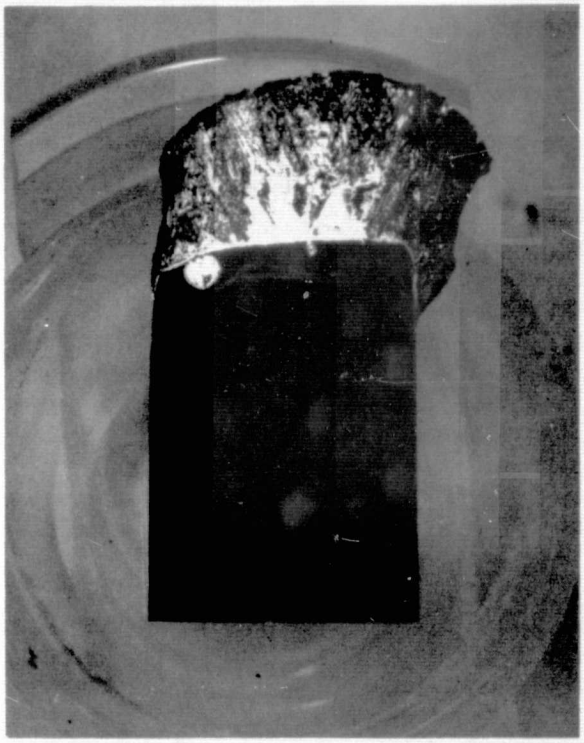

Figure 44. Seeded Growth Obtained During SGF-17. Single-crystal areas having the same orientation as the seed crystal have been highlighted by reflected light. The seed crystal is 11 mm wide.

During these experiments it was noted that electromagnetic stirring had been of little value in promoting crystal growth; therefore, for subsequent experiments the furnace was reassembled without the tungsten electrode. A further modification was the introduction of a water-cooled gas jet as a way of achieving local cooling, combined with the advantages of good visibility near the growth edge.

c. FURNACE CLEANLINESS TESTS

Further surface growth experiments were carried out, but they continued to yield material which was very poor in crystal structure. The poor quality of this growth was believed to be caused by impurity contamination in the furnace, which poisoned the growth interface. Therefore, we introduced a test procedure which proved to be of considerable help in detecting the presence of various sources of contamination.

Etch-polished silicon test wafers were stripped of oxide with diluted HF solution and were then heated in the empty growth furnace for 45 minutes at 1070 °C in hydrogen. They were then removed and measured with an ellipsometer to detect the presence of any film that might have developed on their surfaces. Under clean furnace conditions this test yielded readings of 3 to 4 Å and the test wafer showed no visible traces of haze or staining.

Table XI summarizes the results of an initial series of such tests conducted in the surface growth furnace. The experiments were given successive numbers each time the furnace was assembled for operation. Once assembled, the furnace could be heated several times to carry out cleanliness tests or to grow silicon. These experiments were distinguished by the letters A, B, C, etc. The molybdenum susceptor was used for the first time in Run 15.

Table XI

FILM GROWTH ON SILICON TEST SAMPLES FROM THE SURFACE GROWTH FURNACE

Exp.	Temp (°C)	Time (min)	H_2 Flow (ℓ/min)	t (Å)	Index	Comments
14A	1070	45	10	463	3.13	Hazy, non-specular
14B	1070	45	8	385	1.50	
14C	1070	45	10	7.5	--	
14D	1070	45	10	6	--	
15C	1070	55	6	17	--	
15D	1080	50	6	19	--	
18A	~1000	15	5	16.8	--	Clear surface
18B	1130	15	5	301	1.91	Haze, a few spots
19A	1075	30	6	130	3.5	Spots at one end
19B	1072	30	10	195	2.56	Haze, many spots
20A	1120	30	5	37	--	Clear surface
21A	1070	30	6	14	--	Haze
21B	1080	30	6	-	--	Heavy haze, spots

These tests showed that considerable film growth was taking place, and several steps were taken to eliminate sources of contamination. Water leaks in the cooling jet developed on several occasions, evidently due to the stresses caused by differential expansion. These leaks could not be detected by helium leak detectors but were eventually eliminated by a redesign of the jet assembly. Neoprene O-ring gaskets were used initially to seal the ends of the quartz tube which formed the furnace envelope, but these decomposed during operation of the furnace. This difficulty was solved by replacing the O-rings with indium compression gaskets, which were kept from melting by thermal contact with the water-cooled header plates.

Back-diffusion of air through openings in the exit header was another source of contamination which caused considerable difficulty. The feed-throughs for the thermocouple and electromagnetic stirring electrodes were eliminated. The depth of the exit port was extended by adding a metal duct at the outer face of the exit header and by using a section of rectangular quartz tubing inside the furnace to reduce convection flow in the neighborhood of the exit port. These modifications appeared to eliminate the contaminants which had been responsible for the film growth on the test wafers, and they were incorporated even more effectively in a further furnace redesign (introduced at Run 50) which will be described later.

The improvement in furnace cleanliness resulting from these measures is seen in the results presented in Table XII. With the exit port sealed and hydrogen leaving via the cooling jet line (Test 41A), a reading of 3 Å was obtained, corresponding to negligible film formation. However, a significant film was observed in tests carried out with the exit port open (Tests 42A and B), indicating that back-diffusion of air was taking place. Because of these observations, we redesigned the furnace. The new furnace eliminates all neoprene gaskets and has a much longer exit port, which is further extended by a quartz duct inside the furnace. Tests 50B through 50F, made with the new furnace, show no evidence for any film growth under any of the operating conditions indicated. Test 50C was conducted with the hydrogen leaving via the exit port, and with the normal gas flow of 12 ℓ/min. The flow was reduced to 6 ℓ/min for test 50D, and because there was still no indication of back-diffusion, it is felt that the new design has eliminated the problem.

Table XII

FILM GROWTH ON SILICON TEST SAMPLES
FROM THE SURFACE GROWTH FURNACE

Exp	Notes	H_2 Entry	H_2 Exit	Film Thickness and Appearance
38A	1	Header	Dummy	35 Å, Considerable Haze
39A	2	Header	Jet	7-9 Å, Haze
40A	2	Header	Port	10-11 Å, Haze
40B	2	Header	Port	6 Å, Considerable Haze
41A	2	Header	Jet	3 Å, Clear
42A	2	Header	Port	11 Å, Clear
42B	2	Header	Port	9 Å, Clear
45A	3	Header + Jet	Port	12 Å, Clear
50B	4	Header	Jet	3 Å, Clear
50C	4	Header + Jet	Port	3 Å, Clear
50D	4	Header + Jet	Port	3 Å, Clear
50F	5	Header + Jet	Port	3 Å, Clear

Notes: (1) Graphite susceptor in contact with quartz; jet assembly replaced by dummy header; sapphire tray; graphite ramp

(2) Pt spacer between susceptor and quartz

(3) Mo susceptor; graphite tray

(4) New seeded growth furnace assembly; graphite susceptor

(5) Sapphire tray added

d. FURTHER SURFACE GROWTH EXPERIMENTS

Numerous surface growth experiments were carried out while these sources of contamination were being tracked down and eliminated. The results obtained during this period can be illustrated by the silicon produced during Run 27, which was made using twinned silicon web to initiate growth. Eleven growth experiments were carried out during this run, as shown in Figures 45 and 46.

Figure 45. Silicon Growth Obtained During SGF-27. These results were obtained with a sapphire tray, graphite ramp, and a twinned silicon web seed.

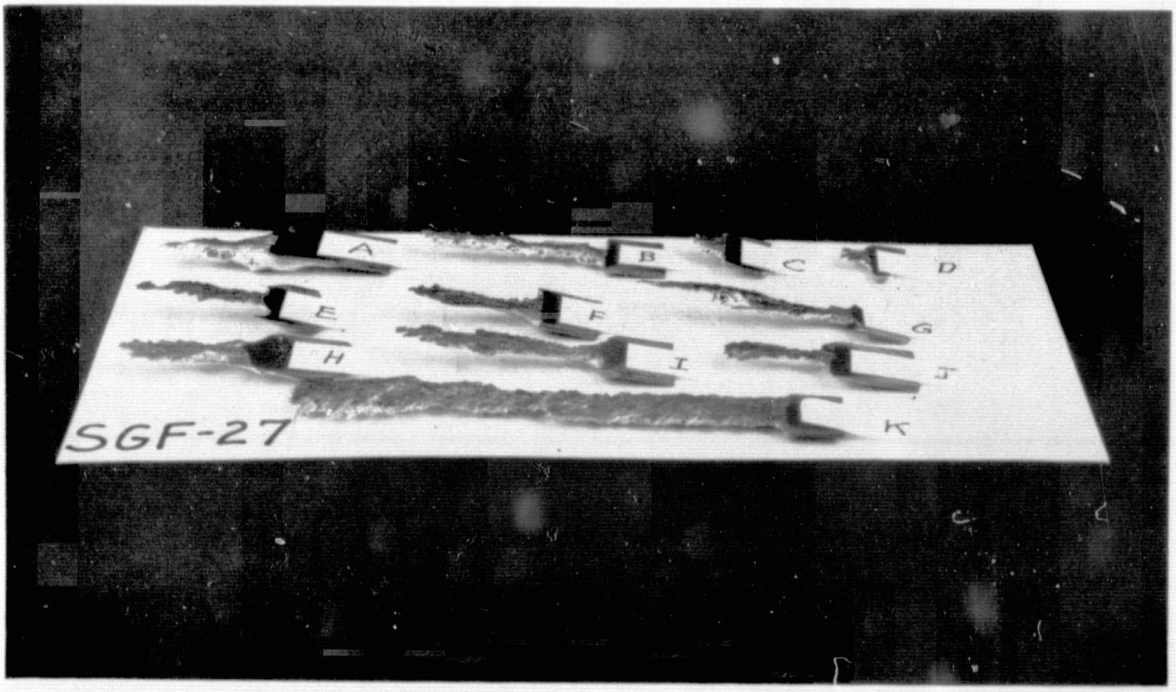

Figure 46. Oblique View of the Growth Obtained During SGF-27

The most successful of these experiments, 27K, produced a strip of silicon 7 cm in length with an average growth velocity of 0.23 cm/min. However, the crystal structure of this silicon was still very poor and showed little evidence of seeded growth. These results implied that crystallization was still being inhibited by the presence of impurities in the melt.

The operation of the surface growth furnace was greatly improved following the elimination of the water leaks in the gas cooling jet and the improved ducting at the exit port. The "skirt," which previously had been observed to form around the silicon charge as it dissolved in the tin, was absent, and there was no longer any significant buildup of deposits within the furnace during operation. These changes made the splicing and growth operations easier to carry out, but they did not result in significantly improved crystal growth.

Run SGF-43 was carried out with a graphite susceptor after the contamination sources mentioned above had been corrected. The preceding test Runs 42A and 42B, shown in Table XII, had revealed bright clean surfaces on the silicon test wafers with 9 to 11 Å of oxide, showing greatly improved cleanliness with only a slight amount of back-diffusion taking place at the exit port. The furnace was then loaded with tin and silicon and operated for three successive days, producing Runs SGF-43A through H. These runs yielded a total of approximately 25 cm of polycrystalline ribbon. The molybdenum heat shields at the left end of the furnace were omitted during these experiments. This limited the operating temperature so that a somewhat lower silicon concentration than normal was used. A nontwinned, <112> oriented seed crystal was used. During these tests the melt remained quite clean, with only a trace of scum at the beginning of each run. The scum appeared to be carried off during the initial portion of each growth experiment, so that the melt surface appeared perfectly clean during most of each growth period. However, the quality of the growth obtained did not appear to be significantly improved over that of previous experiments, such as SGF-27, shown in Figures 45 and 46.

Run SGF-44 using the graphite susceptor and a tray made of tungsten was assembled next. Initial operation with tin only showed that the tin wetted and spread over the tungsten surface. To prevent the tin from creeping up over the edge of the tray, this edge was painted with colloidal graphite, which greatly reduced the creep. Silicon was then added and the furnace was operated to produce SGF-44A, B, G, and H. SGF-44G showed oriented growth which started at several points at the end of the seed crystal and spread out from each point in the form of 60° V-shaped branching patterns. This series was terminated by loss of the graphite barrier, which permitted tin to leak out of the tray.

The furnace was next assembled with the molybdenum susceptor and a graphite tray. After an initial firing to bake out the tray, a silicon test wafer was introduced to evaluate the cleanliness of the furnace atmosphere. With hydrogen introduced through both the furnace inlet and the cooling jet, and leaving via the exit port, an ellipsometer reading of 12 A was obtained. This is consistent with previous experience and implies a slight amount of back-diffusion of air through the exit port. Tin and silicon were then introduced, and Runs 45A through D were carried out. Except for a slight amount of scum, which probably came from the graphite and was carried away by the initial growth, this melt remained bright and clean in appearance throughout these growth experiments. The quality of the growth achieved was similar to that of the previous series.

e. MODEL 3 - NEW SURFACE GROWTH FURNACE

By this period in the program, the surface growth furnace had undergone considerable modification and reworking, and several shortcomings had become evident. A new furnace which eliminated these deficiencies was constructed as shown in Figure 47.

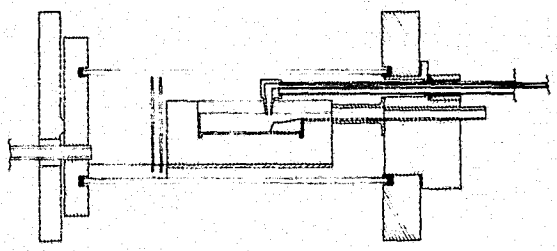

Figure 47. Surface Growth Furnace Having Indium Gasket Seals and Removable Header Block

Indium gaskets were used at all joints to provide clean, vacuum-tight seals. All feed-throughs were eliminated from the headers, for ease of assembly and to eliminate opportunities for leaks. The length of the exit port was greatly extended and its area reduced by an insert, which could be removed in the event it became necessary to remove a large mass of crystal from the furnace. The exit port and cooling jet assembly were contained in a header block, which could be removed to take out the susceptor without breaking the seals at each end of the furnace tube.

This new furnace was operated for Runs SGF-50 through 54. These experiments included a series of silicon test strips, which verified the improved cleanliness of the furnace, and some growth experiments using <112> oriented seed crystals. After some initial difficulty in achieving proper alignment between the exit port and the growth chamber of the furnace, some silicon was grown during SGF-54D. The quality of the growth was not significantly different from that achieved in previous experiments.

f. VERTICAL SEEDED GROWTH FURNACE

The surface growth experiments described above were intended to initiate platelet growth along the free surface of the tin-silicon melt. It is possible that this surface cannot be made sufficiently clean to avoid heterogeneous nucleation at the silicon-melt interface, or that some unrecognized instability associated with growth at the intersections of the solid, liquid, and gas phases prevents single-crystal growth from taking place. On the other hand, it appeared that it might be possible to achieve seeded growth within the melt by dipping a seed crystal into a supercooled melt and drawing it up in a manner analogous to the growth of dendrite ribbons from a pure silicon melt. In this case, the floating substrate concept could be modified so that deposition from silane could be used to maintain supersaturation and to increase the thickness of the silicon to the desired value after it had emerged above the surface of the melt.

The furnace shown in Figure 48 was constructed to explore this possibility. It consisted of a quartz envelope with a graphite susceptor and alumina crucible, which was heated using an induction coil in a hydrogen atmosphere. Tin was placed in a quartz boat in the right arm of the furnace, melted, and allowed to pour through a small capillary into the crucible. Any surface residue that appeared as the tin melted was skimmed off and kept in the boat by a droplet which remained in the capillary. The opposite arm of the quartz envelope contained pellets of etched silicon, which were pushed into the crucible by a magnetic capsule as needed during the experiment. A seed crystal was introduced through the stainless steel header by a pull rod which was blanketed by nitrogen cover-gas to eliminate back-diffusion of air where the pull rod passed through the header. The envelope was sealed to the header with an indium gasket.

Three initial runs with silicon test wafers were made to test the purity of the furnace atmosphere. The first, VSGF-1, employed a graphite crucible which had been used in previous work and was then cleaned by firing to 1700 °C in vacuum. In spite of this cleaning, the test wafer showed some stain and a film thickness of 50 Å.

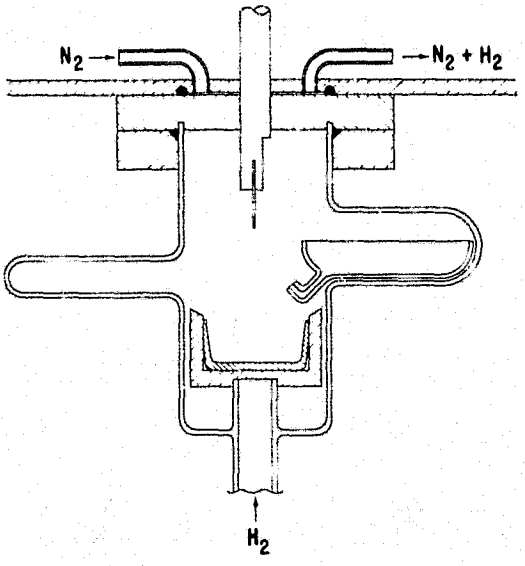

Figure 48. Vertical Seeded Growth Furnace. The crucible is loaded with tin and silicon from the two side arms of the furnace envelope.

In the next run a new crucible that had been similarly vacuum-fired was used. This time the test wafer came out nearly free of stain and showed only 14 Å of film growth. The crucible was then baked out further by heating it in the VSGF furnace in a nitrogen atmosphere for two hours at maximum power, which brought it to 1185 °C. A test wafer made after this bakeout showed only 9 Å of film growth, indicating that the cleanliness of the furnace was considerably improved, although it was still not as clean as it should have been.

After these initial tests, the system was loaded with tin and silicon, and five seeding experiments were carried out. In general, the melt looked bright and clean, with little or no scum appearing on the surface. When silicon was added, it dissolved without any "skirt" forming around its edges, indicating that the system was quite clean. In most of these seeding experiments, twinned seeds cut from web dendrites were used. These were oriented with their re-entrant edges down toward the melt in most cases. An untwinned seed was tried in VSGF-6; in VSGF-7 a twinned seed with inverted orientation was used.

There was no problem with dipping the seed into the melt and achieving a growth of silicon on the end of the seed. However, when the seed was etched free of excess tin and examined, no evidence could be found that any seeded growth had taken place.

The silicon crystals appeared to nucleate at random, with the densest part of the growth appearing where the melt surface met the seed crystal. The submerged end of the seed did not exhibit any preferential growth, such as had been anticipated in the neighborhood of the re-entrant edge of the seed.

g. UNSEEDED SURFACE GROWTH

Platelet growth was often observed to take place on the free surfaces of tin-silicon melts as they were cooled below the liquidus temperature. Examples of such growth are shown in Figures 49 and 50, obtained during supercooling Experiments KB-6 and KB-15.

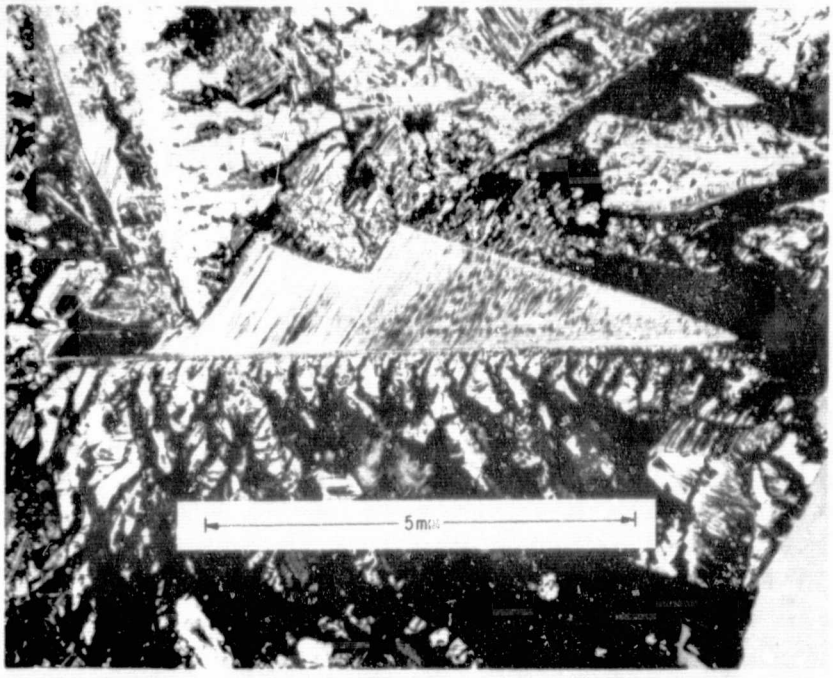

Figure 49. Example of Two-Dimensional Planar Growth produced during KB-6. The dagger shaped crystal grew by itself. The branched dendritic crystals surrounding it developed separately at a later stage of the cooling cycle

Each platelet has a straight "spine" which runs along one edge or down the middle. This is oriented in the <112> direction. The face of the platelet which appeared on KB-6 was approximately a (110) surface, but in the case of the larger platelet from KB-15 it was tilted about 20° off the (110) plane. Evidently the platelet faces are not oriented in any particular crystallographic direction. A set of closely spaced crystals having

Figure 50. Several Examples of Planar Growth from KB-15.

(111) faces grows down into the melt from the underside of each platelet. Their intersections with the free surface of the platelet appear to correspond with the parallel streaks which can be seen on its surface. The larger platelet from KB-15 was broken open so that this parallel growth could be observed more clearly. A photograph of this section is shown in Figure 51. The thickness of the surface crystal is approximately 30 μm while the parallel platelets run about 3 to 9 μm in thickness and are spaced approximately 20 to 40 μm apart.

It is not known whether the parallel growth took place as the surface crystal was being grown or whether it took place during a later period of the cooling process.

Hexagonal crystals 2 or 3 mm in diameter were also observed occasionally during the cooling of these melts. The surfaces of these crystals were quite smooth, indicating that they were highly perfect. They appeared to be similar to those shown in Figures 27 and 28 and, presumably, were able to grow to larger sizes beause of the larger melts and slower cooling rates that were involved.

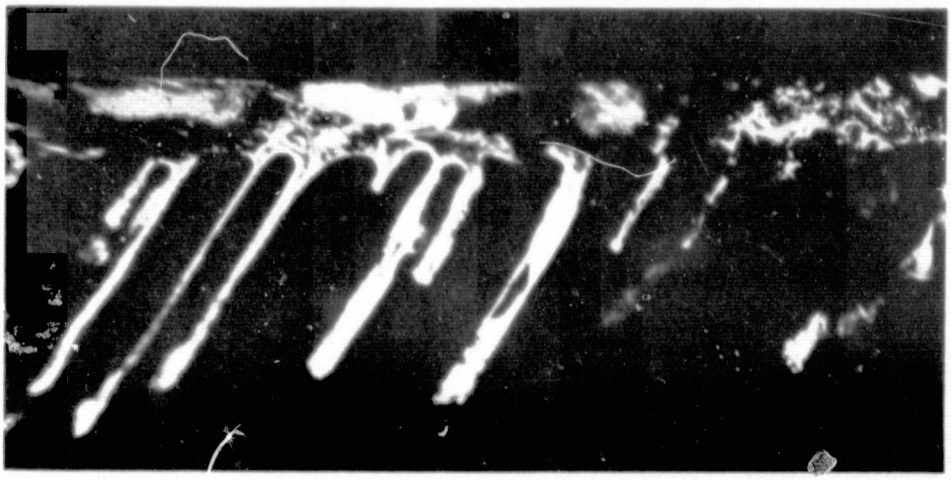

Figure 51. Section of Surface Crystal Growth During KB-15 Showing Parallel Platelet Growth Which Extended Down Into the Melt.

6. CONCLUSIONS

The floating substrate method of crystal growth involves several processes which were studied during the course of this contract. It was found that most of them could be carried out in a manner consistent with the practical realization of silicon sheet growth. However, we were unable to propagate single-crystal growth from the tin-silicon melt, with the result that the crystal structure of the sheet growth obtained was not adequate for semiconductor purposes.

The reasons for the polycrystalline growth are not clear. The most probable cause was thought to be poisoning of the growth interface by impurities, either in solution or on the melt surface. However, measures taken to improve the cleanliness of the furnace did not significantly affect the quality of the silicon produced. These changes included the use of different refractory container materials, graphite vs. molybdenum susceptors, and elimination of air and cooling water leaks. Nitrogen was eliminated from the furnace atmosphere because of indications that it caused a film to form on the surface of tin-silicon melts, but this did not improve the growth characteristics either.

It may be that the change in lattice parameter, resulting from the tin dissolved in the silicon which crystallized from solution, was sufficient to prevent epitaxial growth on the ends of the pure silicon seed crystals used to initiate growth. However, this argument would not apply to the small single-crystal regions which often appeared but did not continue to propagate. These persisted for only a few milimeters and then reverted to dendritic growth.

It seems possible that there may be an inherent instability associated with rapid platelet growth from the tin-silicon solution perhaps due to constitutional supercooling. The small crystallites studied via the sessile drop experiments always started from twinned nucleii and grew rapidly for a short time. Their growth then ceased, and was resumed by branching in other directions. Platelet growth could take place from the re-entrant edges of the dendrite arms, but, since these kept branching off in new directions, the growth of platelets was always interrupted. This same instability may have been responsible for the inability to achieve single-crystal ribbon growth using the floating substrate method.